2021

Transmission-Level Impact Analysis of Utility-Scale Solar Photovoltaic Systems and Battery Energy Storage Grid Support

Gerald W. Bankes II
University of Kentucky, geraldbankes@gmail.com
Digital Object Identifier: https://doi.org/10.13023/etd.2021.464

STUDENT AGREEMENT:

I represent that my thesis or dissertation and abstract are my original work. Proper attribution has been given to all outside sources. I understand that I am solely responsible for obtaining any needed copyright permissions. I have obtained needed written permission statement(s) from the owner(s) of each third-party copyrighted matter to be included in my work, allowing electronic distribution (if such use is not permitted by the fair use doctrine) which will be submitted to UKnowledge as Additional File.

I hereby grant to The University of Kentucky and its agents the irrevocable, non-exclusive, and royalty-free license to archive and make accessible my work in whole or in part in all forms of media, now or hereafter known. I agree that the document mentioned above may be made available immediately for worldwide access unless an embargo applies.

I retain all other ownership rights to the copyright of my work. I also retain the right to use in future works (such as articles or books) all or part of my work. I understand that I am free to register the copyright to my work.

REVIEW, APPROVAL AND ACCEPTANCE

The document mentioned above has been reviewed and accepted by the student's advisor, on behalf of the advisory committee, and by the Director of Graduate Studies (DGS), on behalf of the program; we verify that this is the final, approved version of the student's thesis including all changes required by the advisory committee. The undersigned agree to abide by the statements above.

Gerald W. Bankes II, Student

Dr. Dan M. Ionel, Major Professor

Dr. Daniel Lau, Director of Graduate Studies

Transmission-Level Impact Analysis of Utility-Scale Solar Photovoltaic Systems and Battery Energy Storage Grid Support

---

THESIS

A thesis submitted in partial fulfillment
of the requirements for the degree of
Master of Science in Electrical
Engineering in the College of Engineering
at the University of Kentucky

By
Gerald Bankes
Lexington, Kentucky

Director: Dr. Dan M. Ionel, Professor and L. Stanley Pigman Chair in Power
Lexington, Kentucky 2021

ABSTRACT OF THESIS

TRANSMISSION-LEVEL IMPACT ANALYSIS OF UTILITY SCALE SOLAR PHOTOVOLTAIC SYSTEMS AND BATTERY ENERGY STORGE GRID SUPPORT

Solar photovoltaic energy generation is expected to grow dramatically in coming years in order to take advantage of renewable and clean sources of electricity. This thesis presents research on the impact of increasing solar PV penetration, specifically of large, utility-scale PV facilities, on transmission network performance. The development of Python programming tools for automation of power flow analysis is presented. A modified version of the IEEE 118-Bus test system is developed and modified to simulate increasing PV generation on the transmission system. The impacts on performance are analyzed trends are reported. Battery energy storage systems are studied in this thesis for their ability to regulate system voltages through reactive power support. The modified IEEE test case is used as a basis to present a developed method for optimization of the location of battery systems for voltage support.

KEYWORDS: Photovoltaics, renewables, transmission, battery, energy storage, IEEE 118-Bus test case.

Gerald Bankes

December 17, 2021

Transmission-Level Impact Analysis of Utility-Scale Solar Photovoltaic Systems and Battery Energy Storage Grid Support

By

Gerald Bankes

Dr. Dan M. Ionel
Director of Thesis

Dr. Daniel Lau
Director of Graduate Studies

December 17, 2021
Date

ACKNOWLEDGMENTS

Firstly, I would like to express the deepest gratitude for my advisor Dr. Dan M. Ionel, Ph.D., FIEEE, L. Stanley Pigman Chair in Power, for his constant guidance, encouragement, and support from the moment that I joined the SPARK laboratory and began my graduate studies.

I would also like to express thanks to all of my professors, especially Dr. Yuan Liao and Dr. Joseph Sottile for their teachings in both my undergraduate and graduate studies and for their review and feedback through service on my thesis committee. I am very grateful toward my expert research and industry mentors at LG&E and KU.

I am extremely thankful for Dr. Oluwaseun Akeyo, my excellent research mentor, who was incredibly welcoming to me and provided selfless guidance and assistance in my transition to graduate school, beginning in the lab, and academic and professional work. I would like to also thank all of my colleagues in the SPARK lab for their support and friendship, and for welcoming me as a member of our academic family.

I would like to thank my parents for their constant love and support, for pushing me to achieve what they knew I could, and for showing me to be the person who I am today.

Finally, I want to thank Kyler Laycock. For your love and support through both of our time in graduate school, for your understanding, your thoughts and insights, and for the light you bring to my life by being at my side I will be forever grateful.

Gerald Bankes

November, 2021

The support of Louisville Gas and Electric and Kentucky Utilities, part of the PPL Corporation family of companies, and the University of Kentucky, the L. Stanley Pigman endowment is gratefully acknowledged.

Contents

List of Figures

List of Tables

Chapter 1

Introduction and Problem Formulation

1.1 Problem Formulation and Original Contributions

Solar electricity generation represents one of the most rapidly growing methods for energy production. Research and interest in renewable forms of energy have increased dramatically in recent years to both provide reliable, replenishing sources of electricity, as well as to invest in more environmentally clean forms of generation. This growth in interest, especially in photovoltaic (PV) generation, will result in a growth of the PV industry through the addition of generation both through the traditional supply by electric utilities who choose to invest in PV facilities, as well as through the investment of customers into residential solar installations.

Both the investment in utility solar and residential solar will add to the amount of

available generation on the grid. This generation also represents a change to the more standard form of synchronous machine generation, relying on power electronic technologies to synchronize generation to the grid. These changes will result in significant alterations to the topology and performance of the grid, shifting the distribution of generation from large, remote generation facilities to many smaller, more local sources of energy.

As the amount of electricity sourced from distributed energy resources (DERs) and inverter-based resources (IBRs) grows, as does the impact on the distribution of generation and system behavior. These changes will have significant impact on the performance of the electrical network. As much of the change takes the form of residential solar installations, much of the research has focused on effects on the grid at the distribution level. The distribution level effects will compound as more residential PV is integrated. In addition to this, utility-scale PV plants are becoming more common and are typically interconnected at the transmission level. Because of this, research into the effects of high levels of PV penetration on the transmission level are vital in understanding how PV generation effects the electric grid as a whole and in mitigating potential issues associated with PV generation before possible grid failures.

The research completed in this thesis aims to address these analyses, presenting a study of transmission-level performance impacts due to increasing levels of distributed

PV penetration. The IEEE 118-Bus test system is modified to include a queue of distributed PV facilities whose power injection is increased to simulate increasing generation across the system. The effects on system performance, including voltages, power flows, and generation distribution, are presented and explored.

Possible issues in system performance due to the integration of PV resources include both system voltage variability due to reactive power insufficiency as well as frequency stability issues due to PV intermittency. These issues must be managed in order to ensure power quality and reliability. Battery energy storage systems (BESS) are one proposed solution to these issues.

BESS facilities typically have been placed alongside PV systems for support; however, it is possible that other locations on the network may be better able to provide support for grid voltages. This thesis proposes a method for optimization of combinations of location for battery energy storage systems to support grid voltages. The optimization algorithm forms a realistic subsection of the design space and searches for a locally optimal solution based on system voltage variations.

The original contributions presented and discussed in this thesis are the following:

- The development of a systematic, automated procedure for the integration of PV and BESS installations into th electric power transmission network. The procedures streamline the process of creating network models of PV integration, optimizing the integration of BESS, and simulating and gathering results

from PSS/E. Python software was developed alongside these procedures for automation of generation deployment and model creation (Chapter 3)

- Grid Analysis of impact for different PV penetration levels. The analysis quantified the important relationship between the distributed nature of additional utility-scale generation and power flow in the system (Chapter 4).

- The development of an optimization method for BESS location and rating to provide voltage support. The algorithm searches a realistic subsection of the location space and provides a locally optimal solution for voltage support (Chapter 5).

1.2 Literature Review

Recent research into large-scale interconnection of PV systems focuses on integration at the sub-transmission and distribution levels. Hosting capacity studies are particularly of interest with the increase in popularity of rooftop solar modules. Many methods of evaluating the hosting capacity of distribution systems have been examined, such as Monte Carlo simulation (MCS), probabilistic power flow (PPF), and extensive search of the PV location-size space [4–6]. Other areas of research on hosting capacity includes the study of various constraints on which to base hosting capacity, such as thermal loading and overvoltage [7, 8]. as well as methods for the

optimization of PV system controls and location in order to increase the hosting capacity or distribution efficiency [9, 10].

Transmission level research on large-scale PV integration includes analysis of the fault characteristics of solar PV and other inverter based resources on transmission system [11] and the improvement of utility-scale solar power quality using proposed power converter topologies and controls [12]. As distribution tends to be of greater focus, additional research on the transmission network includes co-modeling of transmission and distribution systems, analyzing the effect on both caused by integration of residential distributed PV generation [13–15].

Battery energy storage systems have been studied alongside PV systems for their ability to mitigate challenges associated with solar energy and support grid operation. Researchers have studied the use of battery systems to regulate grid voltage using various control strategies [16, 17] and to flatten the output power profile of PV facilities due to shading and time-of-day variations [18–21].

Research on battery systems also looks to optimize battery parameters and performance for specific networks and use cases. Battery capacity optimization for microgrids, distribution systems, and individual residential systems have been proposed [22–25]. Methods for optimization of battery power flow controls have also been investigated [26–28]. Additional literature review and citations are provided throughout the chapters of the thesis.

1.3 Thesis Outline

Chapter 1 introduces the research presented in this thesis and includes a review of recent literature to provide a background for the present study. Chapter 2 presents the modeling of power system components used in transmission analysis, covering the theory and mathematical models used to describe power transmission components, various forms of electrical generation, and energy storage. Chapter 3 examines the mathematical methods used for steady-state analysis of power systems. The theory and mathematical representations are then related to the operation of power system simulation software. The development of Python code for automation of transmission system studies is presented. Chapter 4 analyzes the steady-state impact of distributed large-scale PV generation on transmission systems. The IEEE 118 Bus test case was modified to include a queue of multi-megawatt PV facilities; the effects on system bus voltages, power flows, and distribution of generation are explored. Chapter 5 illustrates transmission performance improvements on the developed models which incorporate large-scale PV generation by employing battery energy storage. A method for optimizing the location of batteries for grid voltage support is presented and trends in performance as a function of battery integration are discussed. Chapter 6 concludes with a summary and discussion of the original contributions presented and future work that can be conducted.

Chapter 2

Power System Components

This chapter presents the development of theoretical concepts and mathematical representations used in power system modeling. The various models of power transmission components and forms of generation and energy storage are examined.

2.1 Power Transmission

2.1.1 Transmission Lines

One approach to the analysis of analog circuits involves the modeling of electrical connections using ideal conductors or lumped resistance models to reduce the complexity of analysis. With short lengths of conductor, the resistive, capacitive and inductive effects are insignificant compared to those of the circuit components, and can be ignored for simplicity without impact to accuracy. Analysis of transmission lines requires the inclusion of such effects to accurately describe their behavior.

Transmission lines form a two-port network whose behavior can be expressed

using a matrix equation relating the voltage and current at the receiving end of the line to those at the sending end of the network [29]. At the receiving end of the transmission line, the output voltage and current are represented as a vector of the two components V_r and I_r. Likewise, the unknown sending end voltage and current can be represented as a vector of the two components V_s and I_s. A two-by-two transformation matrix can thus be defined to relate these two vectors. The four parameters of the transformation matrix, labeled A, B, C, and D, define the behavior of the network and the relationship between the sending end and receiving end parameters. Using this matrix, the relationship is represented as

$$\begin{bmatrix} V_s \\ I_s \end{bmatrix} = \begin{bmatrix} A & B \\ C & D \end{bmatrix} \begin{bmatrix} V_r \\ I_r \end{bmatrix}. \tag{2.1}$$

The ABCD parameters can be calculated for various models of the transmission line by deriving a set of equations to match the form of the matrix equation, allowing for simplified calculations of voltages and currents according to the selected model.

The material composition and spacial position of transmission lines give rise to several distributed properties of the line visualized in Fig.2.1. The resistance of a material with uniform resistivity (ρ) and cross-sectional area (A) is calculated $\frac{\rho l}{A}$, where l represents the length of the material. The distributed parameter of the transmission line related to its resistance is defined as the resistance of the line divided by the length and is denoted r. The parameter is represented as a series resistance distributed along the transmission line. The position of the transmission line relative

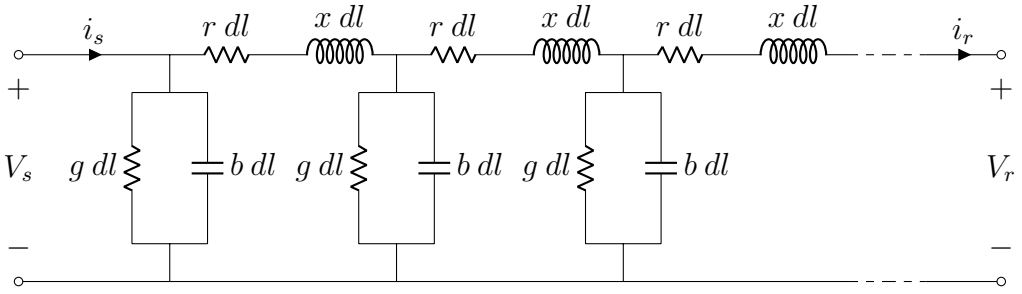

Figure 2.1: The two-port network model for a transmission line with distributed parameters. The distributed resistance (r), reactance (x), conductance (g), and susceptance (b) each represent the associated total value divided along the entire of the line. Values for small lengths of line are represented by multiplying by the differential length dl

to other lines and earth results in inductances and capacitances that must be accounted for. These parameters — defined as x and b respectively — represent the series reactance and shunt susceptance per unit length of transmission line. Finally, leakage current through air or insulating material is represented by the parameter g as shunt admittance, whose effect is typically marginal compared to the transmission line current and is often ignored in certain models.

Three principal models of transmission lines are used for the calculation of the ABCD parameters and are selected based on the length of the transmission line. The long line model is the most detailed, taking into account the distributed nature of the each of the transmission line parameters. The medium and short line models simplify the representation by reducing the distributed parameters into lumped parameters and excluding parameters that may be considered negligible.

The short line model illustrated in Fig.2.2 ignores the negligible effects of current

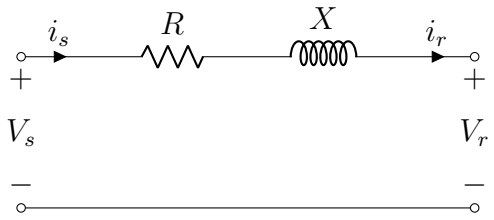

Figure 2.2: The short-line model for a transmission line. This model includes only the effects of the resistance and inductance of the transmission line using the lumped parameters, R and X.

leakage and shunt capacitances on the transmission line. The distributed resistance and inductance are lumped into a single impedance representing the total series resistance and inductance of the entire line. These lumped values are calculated by multiplying the transmission line parameters r and x by the total length of the line. Using Kirchoff's voltage and current laws, the system of equations,

$$\begin{aligned} V_s &= V_r + (R + jX)I_r \\ I_s &= I_r \end{aligned}, \tag{2.2}$$

can be formulated, matching the form of (2.1). By putting these equations in matrix form, the ABCD parameters associated with this model can be calculated. The series resistance and reactance, R and X can be combined as $Z = R + jX$ for simplicity, where Z represents the total series impedance. Thus, the ABCD parameters for this model are

$$\begin{bmatrix} 1 & Z \\ 0 & 1 \end{bmatrix}. \tag{2.3}$$

The medium line model depicted in Fig.2.3 builds upon the short line model by accounting for shunt capacitances on the transmission line that arise from the spacing

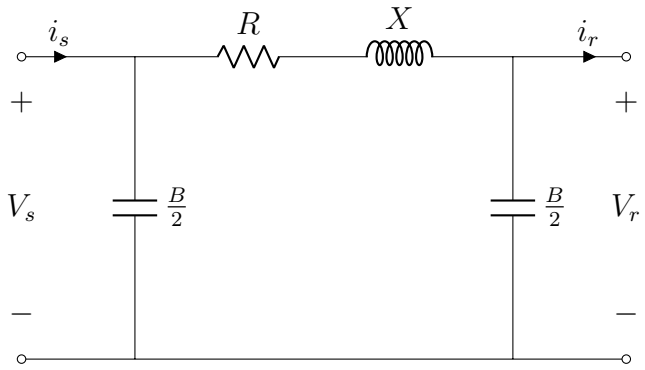

Figure 2.3: The medium-line π model for a transmission line. This model incorporates the effects of the shunt capacitances of the transmission line by distributing the lumped parameter B evenly at the two ends to the line.

between the lines and between the earth. As before, the series resistances and reactances are lumped into a single component representing the total series impedance of the line. The shunt capacitances are also lumped into discrete components; however, the total shunt capacitance of the line, calculated in the same manner as the lumped series impedance, is divided evenly between the two ends of the line. The system of equations defining this model can be derived to be

$$\begin{aligned} V_s &= [\tfrac{(jB)(R+jX)}{2} + 1]V_r + (R + jX)i_r \\ I_s &= (jB)(\tfrac{(jB)(R+jX)}{4} + 1)V_r + [\tfrac{(jB)(R+jX)}{2} + 1]i_r \end{aligned}. \tag{2.4}$$

The series resistance and reactance, R and X can again be combined as $Z = R + jX$ for simplicity where Z represents the total series impedance. Similarly, the total shunt admittance can be represented as $Y = jB$. Thus, the ABCD parameters for this model are

$$\begin{bmatrix} \frac{YZ}{2} + 1 & Z \\ Y(\frac{YZ}{4} + 1) & \frac{YZ}{2} + 1 \end{bmatrix}. \tag{2.5}$$

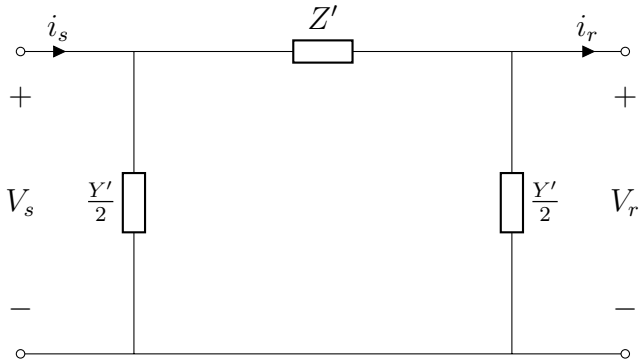

Figure 2.4: The long-line equivalent-π model for a transmission line. The equivalent primed components are calculated from the detailed solution of the differential equation such that the π circuit calculates the same result as the differential equation.

The long line model accounts for the distributed nature of the transmission line parameters and defines equivalent lumped components, Z' and Y', that take these effects into account and can be used in the equivalent-π model. Using a single segment of the distributed transmission line model in Fig.2.1, the system of differential equations,

$$\begin{array}{l} \frac{dV(l)}{dl} = (r+x)I(l) \\ \frac{dI(l)}{dl} = (y+b)V(l) \end{array}, \tag{2.6}$$

can be derived and combined into the single, second-order differential equation,

$$\frac{d^2V(l)}{dl^2} - (r+jx)(y+jb)V(l) = 0. \tag{2.7}$$

The solution of this equation takes the form

$$V(l) = Ae^{\gamma l} + Be^{-\gamma l}, \tag{2.8}$$

where γ is defined as

$$\sqrt{(r+jx)(y+jb)}. \tag{2.9}$$

The current can be calculated from (2.8), $V(0)$ and $I(0)$ are defined as V_r and I_r respectively, and the equations for $V(l)$ and $I(l)$ can be rearranged to match the form of (2.1), resulting in

$$\begin{aligned} V_s &= cosh(\gamma l)V_r + Z_c sinh(\gamma l)I_r \\ I_s &= \tfrac{1}{Z_c} sinh(\gamma l)V_r + cosh(\gamma l)I_r \end{aligned}, \tag{2.10}$$

where Z_c is defined as

$$\sqrt{\frac{r+jx}{y+jb}}. \tag{2.11}$$

Thus, the ABCD parameters for this model are

$$\begin{bmatrix} cosh(\gamma l) & Z_c sinh(\gamma l) \\ \frac{sinh(\gamma l)}{Z_c} & cosh(\gamma l) \end{bmatrix}. \tag{2.12}$$

The ABCD parameters for the long line model and the medium line model can be equated in order to calculate equivalent values of series impedance and shunt conductance which can be used to exactly model the long line using the same π model and is shown in Fig.2.4. Equating the two matrices results in a system of four equations which results in the equivalent parameters being calculated as

$$\begin{aligned} Z' &= Z_c sinh(\gamma l) \\ Y' &= \tfrac{2tanh(0.5\gamma l)}{Z_c} \end{aligned}. \tag{2.13}$$

2.1.2 Transformers

Transformers increase the voltage of transmission lines, reducing current flow and, in turn, resistive losses in the line. The transformer uses electromagnetic induction to scale the voltage level of AC power. An input current flows through a coil of wire,

generates a magnetic field through the coil. The magnetic field is guided by a magnetic core through a second coil of wire, which induces a voltage proportional to the ratio of the number of turns in the first coil to the number of turns in the second. The equivalent-t model of the transformer depicted in Fig.2.5 forms three branches, each representing one of the three components of the transformer: the primary winding, the magnetic core, and the secondary winding. R_1 and X_{l1} represent the resistance of the primary winding and the reactance of the primary winding associated with the magnetic flux which does not link the second coil, also known as the leakage reactance. R_c and X_m represent impedances within the magnetic core, with R_c denoting the resistance of the magnetic core and X_m denoting the reactance in the core linking both the primary and secondary coils. R'_2 and X'_2 represent the resistance and leakage reactance of the secondary wire with reference to the primary side of the transformer. This means that the primed impedance values represent impedances on the primary side that would result in the same current on the primary side as the measured impedances on the secondary side.

2.2 Power Generation

2.2.1 Electromechanical Generation

The traditional method of electricity generation uses external sources of motion (typically the movement of steam) to drive a turbine which is fed to a synchronous AC

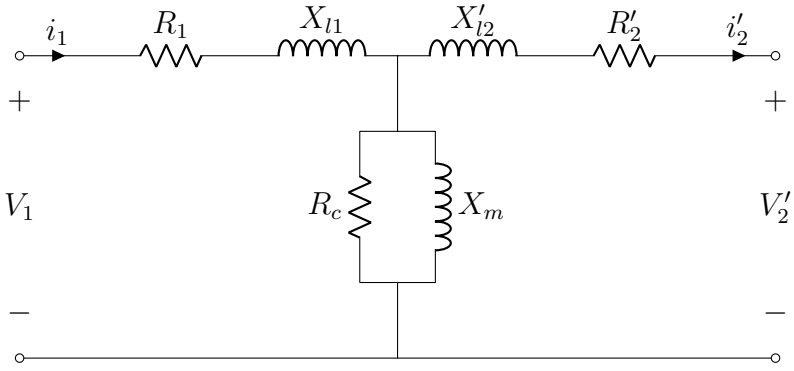

Figure 2.5: Equivalent-t model for a transformer. The series branches represent the impedances associated with the primary and secondary windings. The shunt components represent the losses due to the magnetic core

generator. For the AC generator to produce electricity, there must be a mechanical input in the form of rotational motion of the shaft and a magnetic field generated by a winding fed by a DC generator connected to the shaft. These two parameters can be manipulated to control the output of the generator. These two values are controlled by the governor and exciter respectively. The control of the synchronous machine using these two components ensures the generator is able to maintain a voltage and power output set point.

The frequency of the power system is an indication of the mismatch between supply and demand of electricity. In the case where there is a surplus of energy generation, the excess power is converted to kinetic energy in the synchronous machine, resulting in an increase in the speed of the generator and, in turn, an increase in the frequency from its nominal value. The opposite is true in the case of a shortage of generation. The governor system monitors the frequency of the grid in order to detect

power mismatch and adjusts turbine intake to regulate the input mechanical power.

The output voltage of the synchronous generator is controlled by the excitation system. The exciter consists of a DC generator attached to the shaft of the synchronous machine, which provides the excitation field for the machine. This system monitors the output voltage of the generator, varying the supplied field in order to maintain constant output voltage.

2.2.2 PV Generation

Solar PV cells are made through the connection of a P-type and N-type doped semiconductor material forming a PN junction. The junction is able to convert incident photons into moving charge carriers through the photoelectric effect. At the junction, the free electrons and holes combine, forming an electric field from the N-type to the P-type semiconductor. The combining of electron-hole pairs continues until the electric field is too strong for the electrons to cross into the P-type semiconductor. This forms a depletion region at the boundary where no free electrons or holes can be found. When light reaches the depletion region, electrons may be excited and reform the original electron-hole pairs. The electric field of the depletion region causes electrons to move back to the N-type semiconductor and holes to move to the P-type semiconductor. This generates a potential difference between the P and N type semiconductors, which can be connected to drive a current [30].

Due to its formation from a PN junction and its primary current generated by light energy, the two principle components of the PV cell current-voltage (IV) characteristic curve are the irradiance current and the current associated with the PN junction, which is governed by the Schockley equation. The ideal solar cell can thus be modeled as a current source representing the irradiance current in an anti-parallel configuration with a diode. The equation

$$I = I_{irr} - I_s[e^{\frac{qV}{kT}} - 1] \tag{2.14}$$

represents the IV characteristic equation of the ideal solar cell with I representing the output current, I_{irr} the irradiance current, I_s the saturation current, q the electron charge, k the Boltzmann constant, T the temperature, and V the output voltage. A more accurate model in Fig.2.6 is governed by

$$I = I_{irr} - I_s[e^{\frac{q(V+IR_s)}{nkT}} - 1] - \frac{V + IR_s}{R_{sh}} \tag{2.15}$$

and takes into account the internal resistances of the cell [1].

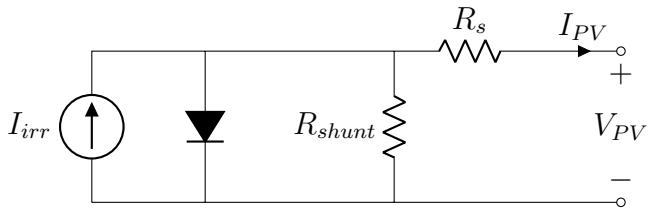

Figure 2.6: The equivalent model of a PV cell based on the IV characteristic equation incorporating internal resistances to model losses within the panel.

The I-V characteristic of the PV cell is primarily dependent on the irradiance reaching the cell and the operating temperature. The amount of light reaching the

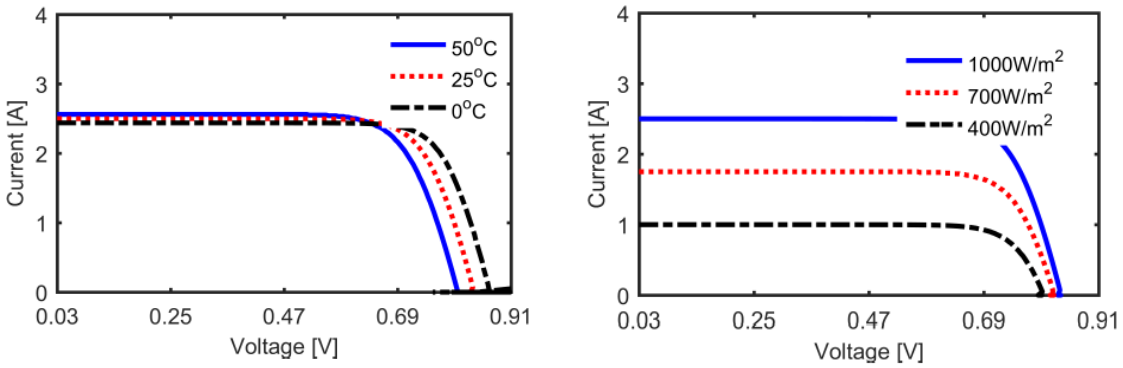

(a) (b)

Figure 2.7: IV characteristic curves of a PV cell and the dependencies on (a) the cell operating temperature (b) the irradiance reaching the cell. The maximum power points occur at the knees of each of these curves [1].

PN junction determines I_{irr} in the IV characteristic. Increasing the irradiance on the solar cell results in a higher current at a specified voltage. The operating temperature has a significant impact on the PN junction voltage in the solar IV characteristic. Increases in temperature results in a lower voltage at a specified current. From this, it can be said that both increases in irradiance and decreases in temperature result in an increase in the power output of the solar cell.

In order to increase the capacity of the a photovoltaic system, individual cells are placed in series to increase the voltage output and in parallel to increase the current output. The combination of cells forms a single solar panel and multiple panels can be connected in the same way to form a higher power PV array.

As PV cells produce DC current, the PV array must connected to the grid using an inverter to convert the DC current into an AC current at the grid frequency. The

inverter uses pulse-width modulation to control switches, which produce a three-phase set of voltages with a fundamental frequency equal to the grid frequency. Filters are used at the output of the inverter to remove the high frequency components of the output waveform introduced by the switching. This results in a nearly sinusoidal output waveform generated from the DC input. The inverter also is able to perform the secondary function of maximum power point tracking. This process ensures that the PV system is operating at the point on the IV curve that produces the most output power. Altering the operating point is achieved by altering the impedance of the system at the terminals of the PV system. This is done by altering the switching of the inverter to effectively alter the impedance seen at the terminals of the PV system.

2.2.3 Battery Energy Storage

The growth in demand for clean sources of energy has led to an increase in the penetration of renewable energy to the transmission system. The most common forms of renewable energy generation, wind and solar, suffer from the issue of intermittency. Battery energy storage systems are one proposed method of mitigating generation intermittency characteristic of solar PV installations. In times of high renewable generation, batteries are able to store excess energy, which can then be discharged during periods of intermittency, flattening out the generation profile of the combined

system.

Batteries store the chemical energy of the bonds between atoms of a substance. Electrochemical cells take advantage of oxidation-reduction reactions, which require the exchange of electrons between substances. By providing a salt path to allow the two substances to react with each other and a conducting path to allow the electrons to be exchanged, the reaction will proceed, and a current through the conductor will be generated.

The voltage output of the battery can be modeled as near constant during normal operation and is a function of the state of charge (SoC) of the battery. The state of charge is the ratio of the charge stored in the battery to the maximum possible charge. For the majority of values of SoC, the voltage output remains near constant; however, near full charge, the voltage is slightly higher than the constant voltage and near zero charge results in a steep voltage drop-off to zero.

Similarly to PV cells, individual batteries can be placed in series to increase the voltage output and in parallel to increase the current output. Battery modules typically are made of a number of cells placed in series and parallel to increase the power output of the module.

Chapter 3

Steady-State Analysis and Software

3.1 Power Flow Formulation

The growth in the integration of renewable energy sources into the electrical grid has led to rapid change in the configuration and performance of the power network. Deployment of distributed energy resources, such as rooftop solar PV installations, has altered the framework for electricity generation by shifting from the model of large, remote generating facilities to many smaller points of generation. The increase in the use of inverter and power electronics-based energy resources leads to a decrease in system inertia, requiring novel methods of mitigation to ensure generation is able to meet demand [31–33]. As these changes are made, analysis of their effect on the system is necessary to ensure power quality and reliability.

Transmission power flow modeling analyzes the steady-state behavior of the transmission network. The network is represented as a graph whose vertices represent

voltage buses and whose edges represent power transmission components; typically transmission lines and transformers. Transmission voltage buses are the sites containing the power generation components and load components and typically represent an aggregate generation and load on at substation.

For the purposes of power flow analysis, transmission system buses are divided into three categories based on the specified and variable quantities at that bus. The four quantities that are used to completely describe the power flow in a network are the voltage magnitude, voltage angle, the real power injection, and the reactive power injection at each bus. Each type of bus has two of these quantities specified and two quantities left variable to be calculated by the solver. Generation buses are directly connected to a source of electrical power and may or may not have a load connection. These buses have known voltage magnitude and real power output and unknown voltage angle and reactive power output. Load buses contain only electrical load and have known real and reactive power output and unknown voltage magnitude and angle. One bus within a transmission area is designated the slack bus, typically a generation bus with a large real power capacity in order to account for generation mismatches. This bus has known voltage magnitude and angle and unknown real and reactive power output.

In order to derive a relationship between the bus voltages and the injected complex power, the relationship between bus voltage and injection current is first defined. The

Bus type	Known Quantities	Unknown Quantities
Slack Bus	V and δ	P and Q
Generator Bus	V and P	δ and Q
Load Bus	P and Q	V and δ

Table 3.1: The three types of transmission system buses and their associated specified and variable quantities.

bus admittance matrix provides this relationship between the total current injected to network buses and the bus voltages. This matrix is derived using Kirchoff's current law at each of the system buses. This results in a system of equations, which is expressed in matrix form as

$$\mathbf{I} = \mathbf{YV}, \tag{3.1}$$

where the admittance is determined as

$$\begin{bmatrix} Y_{11} + Y_{12} + ...Y_{1n} & -Y_{12} & \dots & -Y_{1n} \\ -Y_{21} & Y_{21} + Y_{22} + ...Y_{2n} & \dots & -Y_{2n} \\ \vdots & \vdots & \ddots & \vdots \\ -Y_{n1} & -Y_{n2} & \dots & Y_{n1} + Y_{n2} + ...Y_{nn} \end{bmatrix}. \tag{3.2}$$

Elements of the matrix are calculated using physical network admittance values; however, individual elements within the matrix do not represent quantities with physical significance. Diagonal elements, $Y_(kk)$, of the matrix are calculated as the summation of every admittance connected to bus k. Off diagonal elements $Y_(kn)$, are taken to be the negative of the total admittance between buses k and n.

Using this, the complex power injected into system buses can be calculated as

$$\mathbf{S} = \mathbf{VI}*. \tag{3.3}$$

and when divided into two equations representing the real and imaginary components of **S**, results in the power flow equations,

$$\begin{aligned} P_k &= V_k \sum_{n=1}^{N} V_n[G_{kn}cos(\delta_k - \delta_n) + B_{kn}sin(\delta_k - \delta_n)] \\ Q_k &= V_k \sum_{n=1}^{N} V_n[G_{kn}sin(\delta_k - \delta_n) - B_{kn}cos(\delta_k - \delta_n)] \end{aligned} \tag{3.4}$$

, which relate the real and reactive power injection at each bus to the voltage magnitudes and angles. As a set of nonlinear equations, iterative methods must be used to solve the power flow problem.

3.2 The Gauss-Seidel Method

The Gauss-Seidel method is an iterative technique used to solve linear systems of equations of the form

$$\mathbf{y} = \mathbf{A}\mathbf{x}. \tag{3.5}$$

whose solution is given by

$$x_k(i+1) = \frac{1}{A_{kk}}[y_k - \sum_{n=1}^{k-1} A_{kn}x_n(i+1) - \sum_{n=k+1}^{N} A_{kn}x_n(i)] \tag{3.6}$$

As the power flow equations are nonlinear in nature, a solution cannot be found using linear methods without accounting for the nonlinearity. Using the bus admittance matrix, the power flow of a transmission system can be represented as system of linear equations relating the current injected by system buses to the bus voltages.

To account for nonlinearity, The injection current for a given bus is calculated for each iteration as

$$\tilde{I}_k = \frac{P_k - jQ_k}{\tilde{V}_k^*} \tag{3.7}$$

. The calculated value for current is then used in in the linear equation and the Gauss-Seidel method can be applied to solve. Applying the Gauss-Seidel method to the linear power system equation results in

$$\tilde{V}_k(i+1) = \frac{1}{Y_{kk}}[\tilde{I}_k - \sum_{n=1}^{k-1} Y_{kn}\tilde{V}_n(i+1) - \sum_{n=k+1}^{N} Y_{kn}\tilde{V}_n(i)] \tag{3.8}$$

, an iterative equation, which solves for bus voltage phasors [29, 34].

3.3 The Newton-Raphson Method

The Newton-Raphson method is an iterative technique used to solve nonlinear systems of equations of the form $\mathbf{y} = \mathbf{f}(\mathbf{x})$. The matrix equation is approximated using a first order Taylor series expansion about an initial estimate of the unknown variables.

$$\mathbf{y} = \mathbf{f}(\mathbf{x_0}) + \frac{d\mathbf{f}}{d\mathbf{x}}|_{\mathbf{x}=\mathbf{x_0}}(\mathbf{x} - \mathbf{x_0}) \tag{3.9}$$

The matrix of derivatives denoted $\frac{df}{dx}|_{x=x_0}$, called the Jacobian matrix, is represented as $\mathbf{J}$ and is formed as follows:

$$\begin{bmatrix} \frac{\partial f_1}{\partial x_1} & \frac{\partial f_1}{\partial x_2} & \cdots & \frac{\partial f_1}{\partial x_n} \\ \frac{\partial f_2}{\partial x_1} & \frac{\partial f_2}{\partial x_2} & \cdots & \frac{\partial f_2}{\partial x_n} \\ \vdots & \vdots & \ddots & \vdots \\ \frac{\partial f_n}{\partial x_1} & \frac{\partial f_n}{\partial x_2} & \cdots & \frac{\partial f_n}{\partial x_n} \end{bmatrix}$$

Rearranging the Taylor series approximation results in

$$\begin{aligned} \mathbf{x} - \mathbf{x_0} &= \mathbf{J}^{-1}(\mathbf{y} - \mathbf{f}(\mathbf{x_0})) \\ \Delta\mathbf{x} &= \mathbf{J}^{-1}\Delta\mathbf{y} \end{aligned}, \tag{3.10}$$

which calculates the change in input variables which will shift the estimate of the output values toward the true values of the function. When used with an initial estimate of input and output values, this process can be iterated to solve the nonlinear system of equations.

When applied to the power flow equations, the Newton-Raphson method is represented by the following equation.

$$\Delta \begin{bmatrix} \delta \\ \mathbf{V} \end{bmatrix} = \mathbf{J}^{-1}\Delta \begin{bmatrix} \mathbf{P} \\ \mathbf{Q} \end{bmatrix} \tag{3.11}$$

The power mismatch, $\Delta \begin{bmatrix} \mathbf{P} \\ \mathbf{Q} \end{bmatrix}$ represents the difference between the true values of real and reactive power injection and the values at the current iteration. When multiplied by the inverse of the Jacobian, the mismatch matrix will estimate the change necessary to move the estimated unknown variables toward the true solution.

The iterative process for the Newton-Raphson method consists of the following main steps:

1. An initial estimate of the unknown variables, δ and V, are made for each bus in the network. These values are typically 1 pu for voltage magnitudes and 0° for voltage angle unless estimates of the true values are available. Known values of voltage and angle are set to the specified values.

2. The real and reactive power injected at each bus is calculated from voltages and angles using equation 3.4.

3. The power mismatch at each bus is calculated. For the slack bus, the real and reactive power mismatch is set to zero to support the desired voltage and angle. For generator buses, the real power mismatch is calculated and the reactive power mismatch is set to zero to support voltage magnitude. If the calculated reactive power lies outside of its limits, the reactive power is set at its limit and is then treated as a load bus. For load buses, the real and reactive power mismatches are both calculated.

4. The Jacobian matrix is calculated by differentiating equation 3.4 and using the current voltages and angles.

5. The necessary changes in the voltages and angles are calculated using equation 3.11. Slack bus voltage and angle are left at their specified values. Generator bus voltage is left at it specified values. The calculated changes are applied to generator bus angles and load bus voltages and angles, resulting in the new

estimate for these unknown quantities.

6. The iterative process is repeated from step 2 until the total power mismatch falls below a specified threshold.

3.4 Steady-State Analysis in PSS/E®

PSS/E® is a widely used software tool for power-flow analysis of transmission systems. The software is able to be operated using either a command line interface or a graphical user interface for entry of transmission network information and power flow solution analysis.

3.4.1 Power Flow Solution Methods

PSS/E® has the capability of solving the power flow of a transmission network using five different algorithms: Gauss-Seidel, Modified Gauss Seidel, Newton-Raphson, decoupled Newton-Raphson, and fast-decoupled Newton-Raphson. The Gauss-Seidel and Newton-Raphson methods are performed as outlined in the previous section [35]. Several modifications are made to the Newton-Raphson method in order to significantly reduce computational complexity and run time, resulting in the decoupled and fast-decoupled Newton-Raphson methods.

The Jacobian matrix can be represented in a simplified form, demonstrating four fundamental relationships between bus voltages and power injection: $P-\delta$, $P-V$, $Q-$

δ, and $Q-V$. Of these four relationships, the $P-\delta$ and $Q-V$ form a relationship with a very strong correlation, whereas the $P-V$ and $Q-\delta$ relationships are significantly weaker. The weaker relationships are able to be neglected in the Jacobian matrix, resulting in a set of two decoupled equations which can be solved separately.

$$\begin{bmatrix} \frac{d\mathbf{P}}{d\delta} & \frac{d\mathbf{P}}{d\mathbf{V}} = 0 \\ \frac{d\mathbf{Q}}{d\delta} = 0 & \frac{d\mathbf{Q}}{d\mathbf{V}} \end{bmatrix}$$

$$\begin{aligned} \Delta\mathbf{P} &= \tfrac{d\mathbf{P}}{d\delta}\Delta\delta \\ \Delta\mathbf{Q} &= \tfrac{d\mathbf{Q}}{d\mathbf{V}}\Delta\mathbf{V} \end{aligned} \tag{3.12}$$

Another set of approximations creates a constant Jacobian matrix. This allows the Jacobian matrix to be calculated only once to be used by every iteration. The first approximation states that the expected difference between the angles of buses in the system is very small. Using the small angle approximations for cosine and sine, where $cos(\theta \approx 0) = 1$ and $sin(\theta \approx 0) = 0$ The second approximation states that the susceptance components of the bus admittance matrix are much larger than the admittance components when transmission lines have a large ratio of reactance to resistance. The final approximation states that the reactive power injected to a given bus is much less than $B_{kk}V_k^2$. The resulting Jacobian matrix from these modifications is simply the negative susceptance components of the bus admittance matrix. The injected real and reactive power quantities are divided by the voltage at that bus. This results in a decoupled set of equations with constant Jacobian matrix as shown

below [36, 37].

$$\begin{bmatrix} \frac{\Delta P_1}{V_1} \\ \vdots \\ \frac{\Delta P_n}{V_n} \end{bmatrix} = \begin{bmatrix} -B_{11} & -B_{12} & \dots & -B_{1n} \\ \vdots & \vdots & \ddots & \vdots \\ -B_{n1} & -B_{n2} & \dots & -B_{nn} \end{bmatrix} \begin{bmatrix} \Delta\delta_1 \\ \vdots \\ \Delta\delta_n \end{bmatrix} \tag{3.13}$$

$$\begin{bmatrix} \frac{\Delta Q_1}{V_1} \\ \vdots \\ \frac{\Delta Q_n}{V_n} \end{bmatrix} = \begin{bmatrix} -B_{11} & -B_{12} & \dots & -B_{1n} \\ \vdots & \vdots & \ddots & \vdots \\ -B_{n1} & -B_{n2} & \dots & -B_{nn} \end{bmatrix} \begin{bmatrix} \Delta V_1 \\ \vdots \\ \Delta V_n \end{bmatrix} \tag{3.14}$$

3.4.2 Power Transmission

Power transmission components in PSS/E take the form of either a transmission line or a transformer. Parameters representing the impedances in the models described in chapter three are specified to model the behavior of these components during power flow analysis.

Transmission lines are modeled using the long-line equivalent π-model in Fig.2.4 for power flow analysis [38]. In addition to the buses connected by the line, this requires specification of the per-unit-length series resistance, series reactance, and shunt susceptance of the line. The per-unit-length values are then used to calculate the ABCD parameters for the long-line model using Eqns. 2.12, 2.9, and 2.11. Rearranging the matrix equation describing the ABCD transformation

$$\begin{bmatrix} V_s \\ I_s \end{bmatrix} = \begin{bmatrix} A & B \\ C & D \end{bmatrix} \begin{bmatrix} V_r \\ I_r \end{bmatrix} \tag{3.15}$$

allows the relationship to be represented as an admittance bus matrix, which can

From Bus Number	From Bus Name	To Bus Number	To Bus Name	Id	Line R (pu)	Line X (pu)	Charging B (pu)
1	RIVERSDE 138.00	2	POKAGON 138.00	1	0.030300	0.099900	0.025400
1	RIVERSDE 138.00	3	HICKRYCK 138.00	1	0.012900	0.042400	0.010820
2	POKAGON 138.00	12	TWINBRCH 138.00	1	0.018700	0.061600	0.015720
3	HICKRYCK 138.00	5	OLIVE 138.00	1	0.024100	0.108000	0.028400
3	HICKRYCK 138.00	12	TWINBRCH 138.00	1	0.048400	0.160000	0.040600
4	NWCARLSL 138.00	5	OLIVE 138.00	1	0.001760	0.007980	0.002100
4	NWCARLSL 138.00	11	SOUTHBND 138.00	1	0.020900	0.068800	0.017480
5	OLIVE 138.00	6	KANKAKEE 138.00	1	0.011900	0.054000	0.014260
5	OLIVE 138.00	11	SOUTHBND 138.00	1	0.020300	0.068200	0.017380
6	KANKAKEE 138.00	7	JACKSNRD 138.00	1	0.004590	0.020800	0.005500
7	JACKSNRD 138.00	12	TWINBRCH 138.00	1	0.008620	0.034000	0.008740
8	OLIVE 138.00	9	BEQUINE 138.00	1	0.002440	0.030500	1.162000
8	OLIVE 138.00	30	SORENSON 138.00	1	0.004310	0.050400	0.514000
9	BEQUINE 138.00	10	BREED 138.00	1	0.002580	0.032200	1.230000
11	SOUTHBND 138.00	12	TWINBRCH 138.00	1	0.005950	0.019600	0.005020
11	SOUTHBND 138.00	13	CONCORD 138.00	1	0.022250	0.073100	0.018760
12	TWINBRCH 138.00	14	GOSHENJT 138.00	1	0.021500	0.070700	0.018160
12	TWINBRCH 138.00	16	N. E. 138.00	1	0.021200	0.083400	0.021400

Figure 3.1: The transmission line data spreadsheet of the IEEE 118-Bus test case for input and storage of transmission line information used in PSS/E.

then be factored into the network bus admittance matrix [35].

$$\begin{bmatrix} I_r \\ I_s \end{bmatrix} = \begin{bmatrix} -\frac{A}{B} & \frac{1}{B} \\ C - \frac{DA}{B} & \frac{D}{B} \end{bmatrix} \begin{bmatrix} V_r \\ V_s \end{bmatrix} \tag{3.16}$$

$$\mathbf{Y} = \begin{bmatrix} -\frac{1}{Z_c tanh(\gamma l)} & \frac{1}{Z_c sinh(\gamma l)} \\ -\frac{1}{Z_c sinh(\gamma l)} & \frac{1}{Z_c tanh(\gamma l)} \end{bmatrix} \tag{3.17}$$

Transformers are modeled using the equivalent-t model in Fig. 2.5 for power flow analysis [35]. In addition to the buses connected by the transformer, this requires specification of the total series resistance and series reactance of the transformer, which represents the total impedances of the primary and secondary windings. These values are reported in per-unit values. The impedances supplied for this model can then be placed in the bus admittance matrix for power flow analysis. The transformer

From Bus Number	From Bus Name	To Bus Number	To Bus Name	Id	Specified R (pu or watts)	Specified X (pu)	Magnetizing G (pu or watts)	Magnetizing B (pu)
5	OLIVE 138.00	8	OLIVE 138.00	1	0.000000	0.026700	0.00000	0.00000
17	SORENSON 138.00	30	SORENSON 138.00	1	0.000000	0.038800	0.00000	0.00000
18	MCKINLEY 138.00	302	PVBUS 13.200	1	0.001690	0.070440	0.00000	0.00000
19	LINCOLN 138.00	303	PVBUS 13.200	1	0.001690	0.070440	0.00000	0.00000
20	ADAMS 138.00	300	PVBUS 13.200	1	0.001690	0.070440	0.00000	0.00000
21	JAY 138.00	304	PVBUS 13.200	1	0.001690	0.070440	0.00000	0.00000
25	TANNRSCK 138.00	26	TANNRSCK 138.00	1	0.000000	0.038200	0.00000	0.00000
29	GRANT 138.00	305	PVBUS 13.200	1	0.001690	0.070440	0.00000	0.00000
31	DEERCRK 138.00	306	PVBUS 13.200	1	0.001690	0.070440	0.00000	0.00000
33	HAVILAND 138.00	307	PVBUS 13.200	1	0.001690	0.070440	0.00000	0.00000
34	ROCKHILL 138.00	308	PVBUS 13.200	1	0.001690	0.070440	0.00000	0.00000
35	WESTLIMA 138.00	309	PVBUS 13.200	1	0.001690	0.070440	0.00000	0.00000
36	STERLING 138.00	301	PVBUS 13.200	1	0.001690	0.070440	0.00000	0.00000
37	EASTLIMA 138.00	38	EASTLIMA 138.00	1	0.000000	0.037500	0.00000	0.00000

Figure 3.2: The transformer data spreadsheet of the IEEE 118-Bus test case for input and storage of transformer information used in PSS/E.

would be added between buses i and j by

1. Adding the series impedance (converted to admittance) to the self admittances, Y_{ii} and Y_{jj}.

2. Subtracting the series impedance (converted to admittance) from the mutual admittances Y_{ij} and Y_{ji}.

The magnetizing susceptance and core conductance may also be specified as needed. The transformer model could then be converted into an equivalent impedance, which would then be added to the bus admittance matrix in the same way as described above.

Bus Number	Bus Name	Id	Code	VSched (pu)	PGen (MW)	PMax (MW)	PMin (MW)	QGen (Mvar)	QMax (Mvar)	QMin (Mvar)	R Source (pu)	X Source (pu)
1	RIVERSDE 138	1	-2	0.9550	0.0000	10000.0000	-10000.0000	0.0000	15.0000	-5.0000	0.000000	1.000000
4	NWCARLSL 13	1	-2	0.9980	0.0000	10000.0000	-10000.0000	0.0000	300.0000	-300.0000	0.000000	1.000000
6	KANKAKEE 13	1	-2	0.9900	0.0000	10000.0000	-10000.0000	0.0000	50.0000	-13.0000	0.000000	1.000000
8	OLIVE 138.0	1	-2	1.0150	0.0000	10000.0000	-10000.0000	0.0000	300.0000	-300.0000	0.000000	1.000000
10	BREED 138.0	1	2	1.0500	379.3843	10000.0000	-10000.0000	-4.4754	200.0000	-147.0000	0.000000	1.000000
12	TWINBRCH 13	1	-2	0.9900	90.0000	10000.0000	-10000.0000	120.0000	120.0000	-35.0000	0.000000	1.000000
15	FTWAYNE 13	1	-2	0.9700	0.0000	10000.0000	-10000.0000	0.0000	30.0000	-10.0000	0.000000	1.000000
18	MCKINLEY 138	1	-2	0.9730	0.0000	10000.0000	-10000.0000	0.0000	50.0000	-16.0000	0.000000	1.000000
19	LINCOLN 138.	1	-2	0.9620	0.0000	10000.0000	-10000.0000	0.0000	24.0000	-8.0000	0.000000	1.000000
24	TRENTON 138	1	-2	0.9920	0.0000	10000.0000	-10000.0000	0.0000	300.0000	-300.0000	0.000000	1.000000
25	TANNRSCK 13	1	2	1.0500	225.0000	10000.0000	-10000.0000	85.4933	140.0000	-47.0000	0.000000	1.000000
26	TANNRSCK 13	1	2	1.0150	325.0000	10000.0000	-10000.0000	57.2334	1000.0000	-1000.0000	0.000000	1.000000
27	MADISON 138	1	-2	0.9680	0.0000	10000.0000	-10000.0000	0.0000	300.0000	-300.0000	0.000000	1.000000
31	DEERCRK 138	1	-2	0.9670	0.0000	10000.0000	-10000.0000	0.0000	300.0000	-300.0000	0.000000	1.000000
32	DELAWARE 13	1	-2	0.9630	0.0000	10000.0000	-10000.0000	0.0000	42.0000	-14.0000	0.000000	1.000000
34	ROCKHILL 138	1	-2	0.9840	0.0000	10000.0000	-10000.0000	0.0000	24.0000	-8.0000	0.000000	1.000000
36	STERLING 138.	1	-2	0.9800	0.0000	10000.0000	-10000.0000	0.0000	24.0000	-8.0000	0.000000	1.000000
40	WEST END 138	1	-2	0.9700	0.0000	10000.0000	-10000.0000	0.0000	300.0000	-300.0000	0.000000	1.000000
42	HOWARD 13	1	-2	0.9850	0.0000	10000.0000	-10000.0000	0.0000	300.0000	-300.0000	0.000000	1.000000
46	W.LANCST 13	1	-2	1.0050	0.0000	10000.0000	-10000.0000	0.0000	100.0000	-100.0000	0.000000	1.000000
49	PHILO 138.0	1	2	1.0250	225.0000	10000.0000	-10000.0000	190.0794	210.0000	-85.0000	0.000000	1.000000

Figure 3.3: The machine data spreadsheet of the IEEE 118-Bus test case for input and storage of generator information used in PSS/E.

3.4.3 Power Generation

All forms of power generation are modeled the same way as machines in PSS/E with minor changes to better represent the form of generation used. In addition to the bus location of the machine, all forms of generation require the specification of four parameters: the scheduled voltage at the bus, the real power output of the generator, the source resistance, and the source reactance. The source resistance and reactance are specified in per-unit and default to the values of 0 and 1 p.u. respectively. The reactive power limits of the generator can be set to provide a maximum and minimum limit of reactive power injection of the generator. The above specifications are sufficient for the modeling of traditional forms of generation, however, additional parameters or changes to the above parameters can be made to

better represent PV arrays and battery systems as sources of energy. One additional parameter of machines in PSS/E is the wind machine parameter, which allows for the control of the reactive power output of a machine using a specified power factor. PV arrays can be better approximated by specifying the machine as a type two wind machine, which sets the reactive power limits based on a minimum power factor. Type one wind machines require specification of the reactive power limits. Type three wind machine set the reactive power output so that the specified power factor is achieved. Battery energy storage systems are modeled as traditional machines with a high source reactance [35].

3.5 Development of Automated Analysis in Python

This section describes new developments made for the research in this thesis. The PSS/E Python toolkit was used to develop several scripts to facilitate the creation of specified transmission network models in PSS/E® and also to facilitate the execution of and data collection for case studies of PV integration to the transmission network.

One of the scripts which was developed to allocate and integrate PV generation as specified into the PSS/E® model is shown in Fig. 3.4

The script begins by creating variable to track the remaining generation left to allocate. Then, the list of PV installations is iterated through and the capacity of each PV plant is compared to the amount of generation remaining to allocate. If

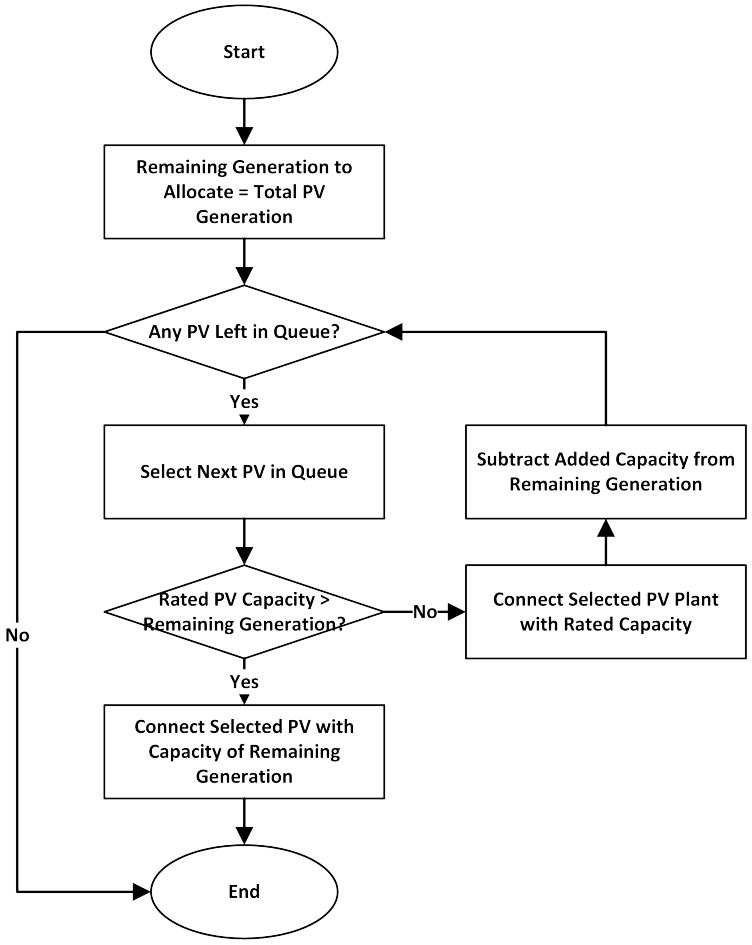

Figure 3.4: Flowchart of the process used for allocating PV generation with a specified total generation in order to simulate future addition of PV facilities over time.

there is more generation to allocate than there is capacity at the current PV plant, the PV plant is connected to the transmission network at its rated capacity and the remaining generation is update by subtracting the rated capacity that was added. The process is repeated until the remaining generation is less then the rated capacity of a generator in the queue. In this case, the PV plant is added at a lowered capacity, equal to the amount of remaining generation to allocate. The script then ends as all of the specified generation has been added.

Another script was developed to alter the generation characteristics of already integrated PV generation facilities. The flowchart describing this script is shown in Fig.3.5 The script begins by calculating the total available capacity of all PV generation by summing the individual ratings of PV facilities. Then, the requested generation is checked to ensure it lies within the rated capability of all PV generation. The ratio used to scale each PV facility generation is set by dividing the requested generation by the total PV capacity. Each plant is then adjusted by multiplying the calculated ratio by the individual plant capacity. The other forms of generation are then redispatched to math the system load. Once all PV generation has been adjusted, the power flow is solved and the total generation is measured to account for transmission line losses. This total generation is then redispatched to other forms of generation.

Another script was developed to allocate existing traditional forms of generation to

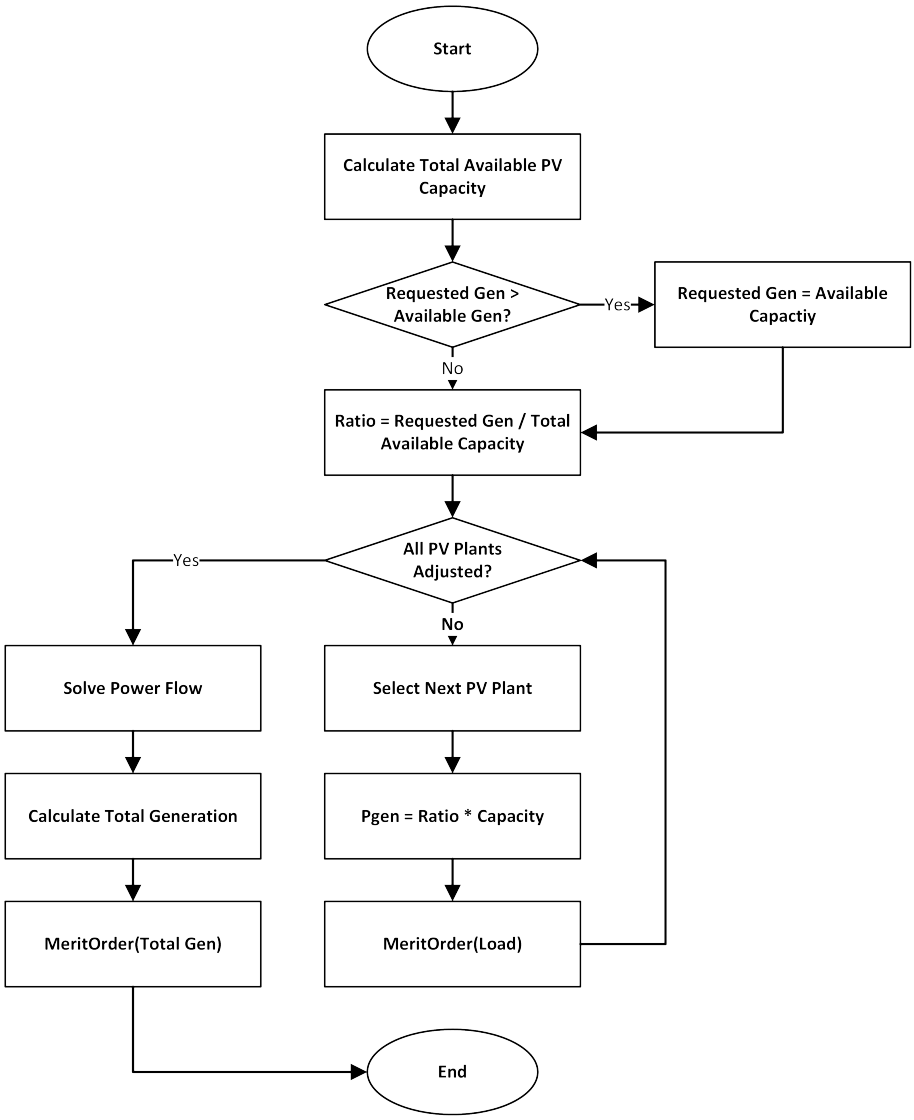

Figure 3.5: Flowchart of the process used for allocating PV generation with a specified total generation by scaling to simulate change in generation of a previously installed fleet of PV generation over time.

match a specified amount of system load while respecting the maximum and minimum power limits of the generator. The flowchart describing operation of the script is shown in Fig. 3.6.

The script begins by initializing a variable to track the remaining amount of generation that has been allocated. The list of generators available for dispatch is then iterated through and the total remaining generation to be allocated is compared to the power limits of the current generator. If the remaining generation is larger than the maximum power output of the generator, the generator is then set to supply power at its maximum limit. The remaining generation to be allocated is then updated by subtracting the added generation from the remaining generation to allocate. If the remaining generation is less than the minimum power output of the generator, then the output of the current generator is set to its minimum power limit. Since more generation was added than was requested, generation must be removed from previously allocated generators. The script then iterates through the list of generators that have been allocated in reverse order. The amount of generation that may be removed while respecting the minimum power limit is checked. If there is more generation to be removed than is allowed for a given generator, the generation is set to the lower power limit and the iteration continues. If all of the surplus generation can be subtracted from a given generator while respecting power limits, the generation is updated and the script ends with all generation allocated. The final condition is

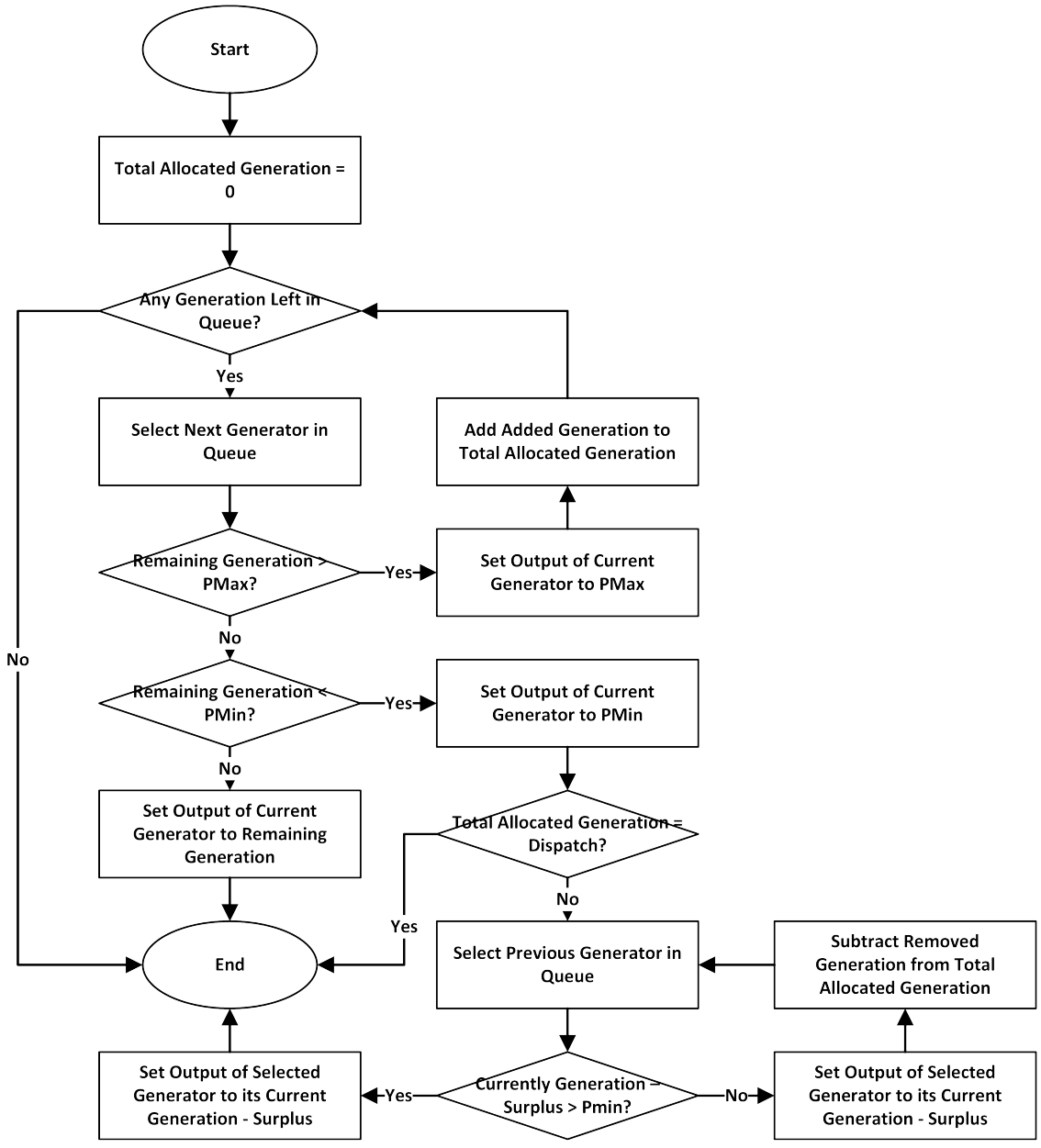

Figure 3.6: Flowchart for the dispatching of existing generating units in merit order, respecting power output limits.

if the total amount of generation remaining to be allocated lies between the power limits of a given generator. In this case, the generation is set to this value and the script finishes with all generation allocated.

These two scripts in combination allow for the automated creation of PSS/E® transmission models of PV integration with specified location and capacity of PV generation, and distribution of traditional generation. A third script was developed to accomplish this as well as allowing for specification of the total amount of load on the transmission network. The script begins by calculating the amount of load in the existing model and creating a scaling factor using the desired load. The scaling factor is applied to each load in the transmission network such that the total load is equal to the desired load. The script continues by using the PV dispatching script described previously to allocate a requested amount of PV generation in specified locations within the model. Finally, the traditional generation allocation script is called to cover system load that was not matched by the added PV generation. The result is a transmission model of a known network whose generation and load are completely specified.

The final script developed was used to determine an optimal configuration of battery energy storage facilities to minimize voltage violations and is described in Fig.3.7 The script begins by initializing the number of violations and previous violations to arbitrarily large numbers to begin the loop. the program checks that the number of

violations has decreased from the previous iteration. The model to be studied is open and the number of voltage violations, previous violations, and the locations of violations are calculated. Each of the locations of voltage violations is tested by adding battery energy storage at the bus. The resulting voltage violations and battery information is recorded and stored in a data structure representing this test loop. Once all locations have been tested, the battery system which results in the fewest voltage violations is selected and connected to the model. The recorded information on this battery configuration is saved to the final program results. This model containing an additional battery is then used as the base model for the next loop to add an additional battery. This process continues until an additional battery does not result in a decrease in the number of voltage violations.

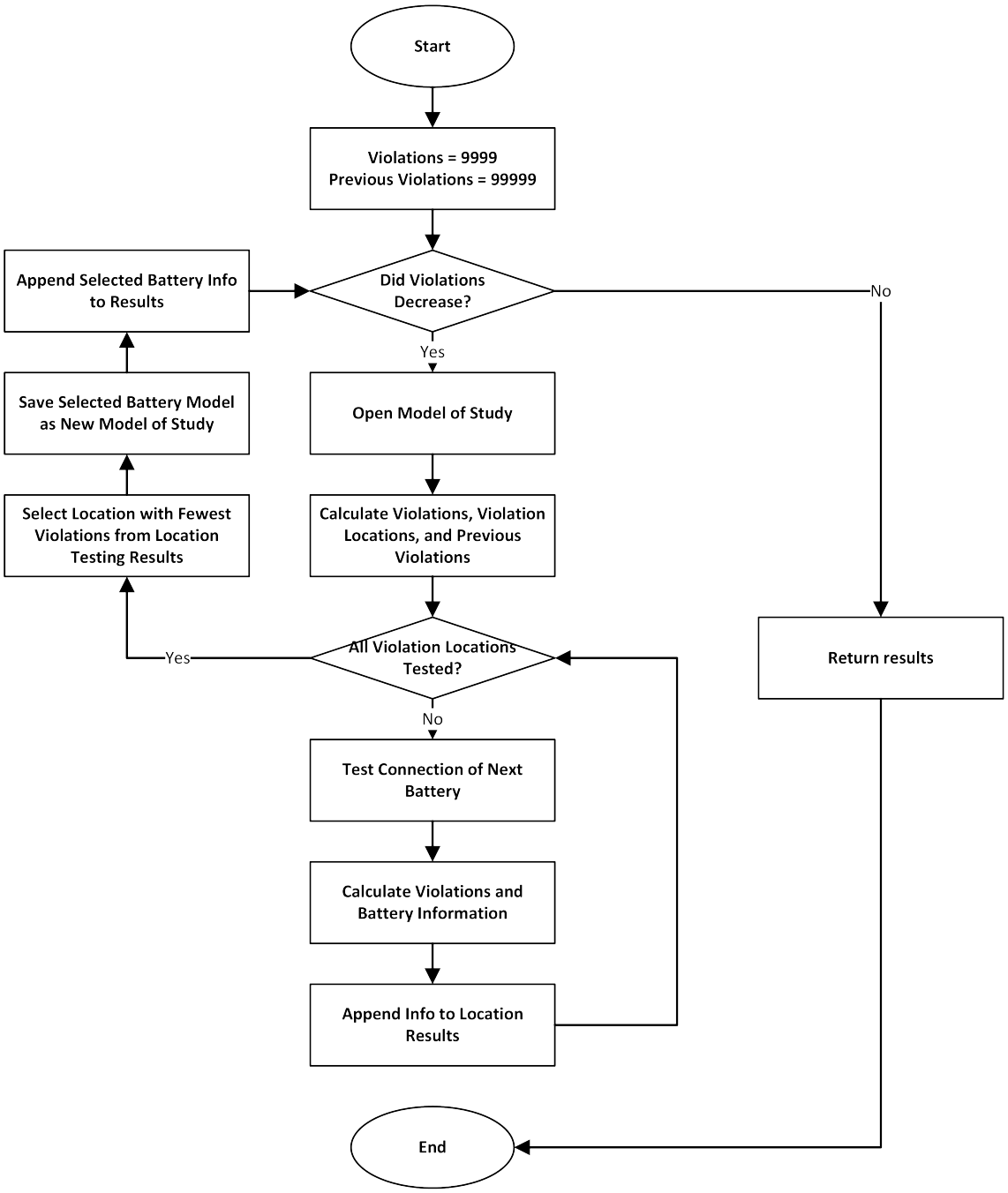

Figure 3.7: Flowchart of the process used for allocating PV generation with a specified total generation

Chapter 4

Case Study on a Modified IEEE 118-Bus Test System

This chapter discusses the simulation of the interconnection of utility-scale solar PV facilities to a representative transmission network using PSS/E. A queue of PV plants was developed for interconnection to the IEEE 118-Bus test transmission network whose output power was incremented to represent increasing levels of PV penetration for impact analysis of large-scale PV systems, which may be applied to real-world transmission systems.

4.1 Introduction

As the dominant source of electricity in the market shifts from fossil fuels to renewable sources of energy, deployment of large-scale PV facilities will move forward at a rapid pace. At the current level of approximately 3% of penetration of solar electricity generation in the market [39], studies on the effect of solar installation

on the electrical grid are chiefly focused on the distribution level. However, the impact of these facilities are not limited to distribution systems. As more distributed photovoltaic generation is incorporated into the distribution system, the effect will propagate to transmission systems. In addition to this, many utilities are looking to develop multi-megawatt scale photovoltaic facilities, which are to be incorporated directly into the transmission network. Thus, studies of the impact of these large-scale penetration levels of PV generation on transmission systems are of critical importance to mitigate possible grid failures before they arise.

4.2 Test Case Specification

Realistic, publicly available models of power system networks are of great need for studies of emerging technology. The IEEE 118-Bus test case was developed in 1962, representing a portion of the United States Eastern Interconnection owned by American Electric Power (AEP). The data for the system was released by AEP for use by the electric utility industry as a standard test case [40]. Since its release as a standard transmission model, several version of the test case have been created with various changes from the original, including increased generation capacity and altered transmission line parameters [41]. The model used for this study was developed by the Illinois Institute of technology in 2004 and was retrieved from the Illinois Center for a Smarter Electric Grid at the University of Illinois. The model consists of 118

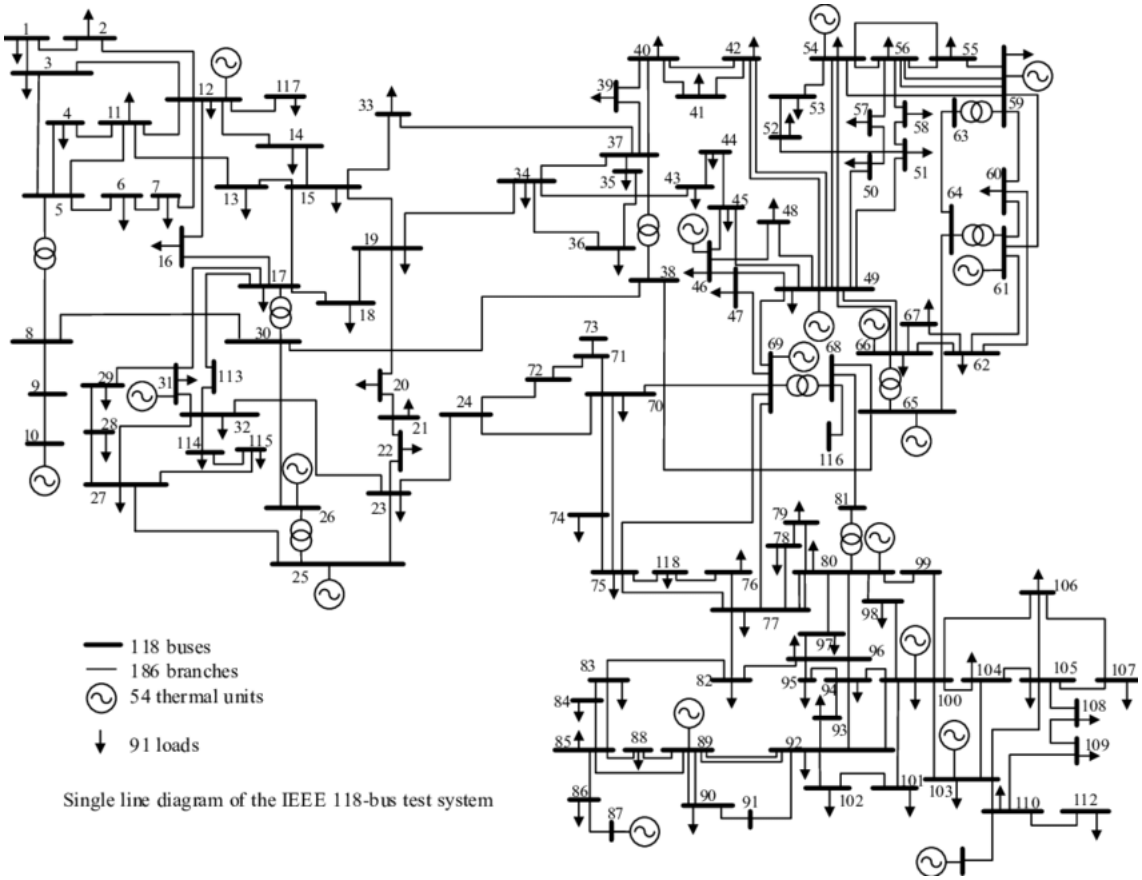

Figure 4.1: Single-line diagram of the IEEE 118-Bus Test case [2].

buses containing 54 generating units and 99 loads. The test case specification contains several buses which experience severe low voltages for the purpose of analysis. For example, buses 40, 41 and 42 experience voltages as low as 0.836, 0.825, and 0.86 p.u. respectively. This low voltage characteristic will be presented in more depth later in this chapter.

In this study, the test system is modified to accommodate the addition of large-scale PV generation through the addition of buses, transformers, and generators which

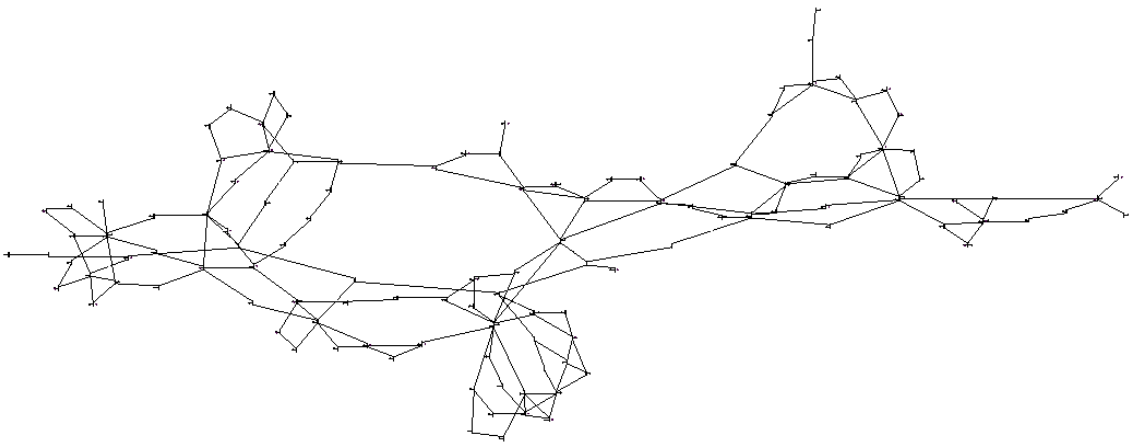

Figure 4.2: Single-line diagram of the test case as produced using the Auto-Draw function in PSS/E and employed in the studies in this chapter.

represent the equipment necessary for interconnection of the PV plants. The existing generation output of real and reactive power is altered to match demand and support the grid voltage.

4.3 PV Array Modeling

Three components are added to the PSS/E model to model the interconnection of a PV array. The first component added to the network spreadsheet is the dedicated PV bus. Two parameters for the bus must be specified: the rated voltage and the bus code. The rated voltage for all PV buses was set to be 13.2 kV. The bus code for PV buses was set to two, representing a generator bus, or P-V bus since both active power and voltage are specified for these buses, in steady-state load flow analysis. For added security in the ability of the solver to find a solution, the angle of the bus was

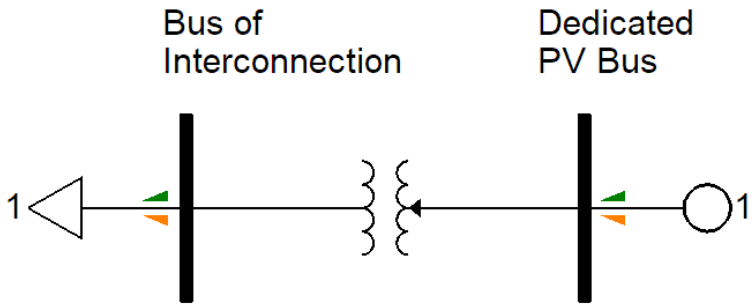

Figure 4.3: PSS/E model for the PV array and its interconnection to the grid. Components added to the original model include the dedicated PV bus, the step-up transformer, and the machine representation of the PV array.

also initialized to be the same value as the angle of the bus of interconnection. By default, PSS/E initializes the angle to zero. Large differences in angle between buses represents a large flow of active power, which may lead to a large power mismatch and the inability of the solver to determine a solution.

The next component is the machine representing the PV generation. Several machine parameters must be specified for the PV generators. The main quantities for load flow analysis are the scheduled voltage output of the generator and the active power output. The scheduled voltage was set to 1 pu and the active power output set to the rating of the PV array. The source impedance of the machine was also specified. For the PV installations, the source resistance was set to 0 pu and the source reactance set to 1 pu. The final parameter of the machine to set is the wind machine value. The wind machine parameter in PSS/E is used for renewable generation facilities as a way to control the reactive power output of these generators.

The wind machine value for the PV plants in the study was set to 2, which limits the reactive power output of the plants to a specified power factor, in this case 0.95.

The final component to be added is the transformer link to the point of interconnection. The resistance and reactance of the transformers were specified. For the PV plants, the resistance was set to 0.001690 pu and the reactance to 0.070440 pu.

4.4 Penetration Study

A queue of PV arrays, denoted PVIcQ (PV interconnection queue), was developed to represent a list of proposed PV interconnections to the transmission network which would result in an increase in the percent PV penetration of the network. Eighteen individual PV facilities were placed in the queue, and the location as well as capacity of each were selected randomly. The location of each facility was selected without replacement from the 118 available buses using a uniform distribution in order to distribute the capacity evenly across the system. The capacity of each facility was selected using a normal distribution with mean of fifty-five megawatts and standard deviation of nineteen megawatts and rounded to a multiple of five megawatts.

The developed Python code was used to create three models of the 118-Bus transmission network with increasing levels of PV penetration. The total system load in the test case was 4,242 MW. Values of PV penetration were selected to be 0, 10, and 20% of the system load. By multiplying the penetration by the system load, the

Position in Queue	Bus of Interconnection	Capacity (MW)	Ic Voltage (p.u.)
1	23	33	0.988
2	58	67	0.958
3	110	67	0.948
4	1	43	0.917
5	97	56	1.006
6	81	51	0.994
7	115	49	0.928
8	30	48	0.944
9	112	56	0.922
10	45	47	0.971
11	37	74	0.920
12	108	72	0.950
13	86	45	0.983
14	28	52	0.919
15	88	70	0.983
16	16	32	0.942
17	47	11	1.013
18	102	40	0.968

Table 4.1: PVIcQ facilities listing the selected bus for interconnection and the rated facility capacity. Interconnection buses were selected randomly without replacement from a uniform distribution. Facility ratings were selected randomly from a normal distribution with a mean of 55 MW and a standard deviation of 19 MW.

Position in Queue	Bus Number	P Max (MW)	P Min (MW)
1	10	450	150
2	80	480	150
3	103	50	5
4	89	650	200
5	111	50	5
6	100	270	110
7	65	400	120
8	66	400	120
9	49	225	100
10	87	12	3
11	69	550	340
12	25	225	100
13	26	325	125
14	59	160	87
15	54	70	10
16	12	90	12
17	61	175	90

Table 4.2: Queue of Merit Order Generation

total amount of necessary PV generation could be calculated and dispatched using the Python program. As the amount of PV generation increases, the corresponding amount of traditional generation must decrease to exactly meet electricity demand. Without reallocation of traditional generation, all of the surplus generation of the system would be removed from the single slack bus, rather than dispatched evenly or economically across the system. As PV is added to the model, the existing traditional generation is reallocated according to a merit order, which acts as a priority queue for generation output.

After the models were created, PSS/E was used to solve the power flow using the

Penetration (%)	Load (MW)	PV Gen. (MW)	Trad. Gen. (MW)	# of Generators
0	4,242	0	4,426.384	17
10	4,242	424.2	4,020.328	13
20	4,242	848.4	3,576.343	12

Table 4.3: System load and generation characteristics for each of the developed models

Fast-Decoupled Newton Raphson method. The solver calculates the voltage at each bus in the network, and from this information, any quantities of interest associated with the power flow may be automatically calculated and returned by PSS/E. The bus voltages, transmission line and transformer power flows, and the generator outputs were all recorded to assess the impact. The trends in these recorded values were analyzed. Typical values of voltage limits from NERC TPL standards are 0.95 and 1.05 per-unit [42]. Limits for transmission line power flow are specific to each line based on heating and ampacity values. The limits for lines in the 118 bus system were not specified.

4.5 Model Validation

After the Python scripts were used to create each of the models of penetration, the files where opened in PSS/E to check that all components were connected correctly and that the models matched the desired generation characteristics. The network spreadsheet in the user interface was used to check each of the added components. Firstly the machines were checked to ensure each of the PV machines were added

with the correct parameters. The transformers were then checked to ensure the PV facilities were correctly interconnected to the network. Lastly, the PV buses were checked to ensure the correct type code was used. The generation characteristics of the model were checked by recording the real power output of the PV and traditional generators in the solved model. The recorded outputs for the PV real power output are shown in Figs. 4.4, 4.5, and 4.6. The total generation was calculated to ensure the penetration level matched the requested value for each model. the traditional generation was also checked to ensure the correct execution of the dispatch code as well as that the total generation roughly matched load. The total generation is slightly higher than the total load as transmission line losses must be accounted for in generation.

4.6 Results

All of the facilities in the PVIcQ were connected to the IEEE 118-Bus test case and their power outputs were scaled to represent 0, 10, and 20% penetration of the load. The base case of no PV generator output was used as a point of comparison between the measurements for each of the levels of penetration.

The distance between each bus in the network and its nearest point of generation was recorded at each penetration level to monitor how the changes to the distribution of generation reflect on the network. Fig.4.4 shows the distance for each bus to

Position in Queue	Bus of Interconnection	Capacity (MW)	PGen (MW)
1	23	35	0
2	58	70	0
3	110	70	0
4	1	45	0
5	97	55	0
6	81	50	0
7	115	50	0
8	30	45	0
9	112	55	0
10	45	45	0
11	37	75	0
12	108	70	0
13	86	45	0
14	28	55	0
15	88	70	0
16	16	30	0
17	47	15	0
18	102	40	0
		TOTAL	0

Table 4.4: PVIcQ facility generation in the 0% penetration case.

Position in Queue	Bus of Interconnection	Capacity (MW)	PGen (MW)
1	23	35	16.14
2	58	70	32.28
3	110	70	32.28
4	1	45	20.75
5	97	55	25.36
6	81	50	23.05
7	115	50	23.05
8	30	45	20.75
9	112	55	25.36
10	45	45	20.75
11	37	75	34.58
12	108	70	32.28
13	86	45	20.75
14	28	55	25.36
15	88	70	32.28
16	16	30	13.83
17	47	15	6.92
18	102	40	18.44
		TOTAL	424.20

Table 4.5: PVIcQ facility generation in the 10% penetration case.

Position in Queue	Bus of Interconnection	Capacity (MW)	PGen (MW)
1	23	35	32.28
2	58	70	64.55
3	110	70	64.55
4	1	45	41.50
5	97	55	50.72
6	81	50	46.11
7	115	50	46.11
8	30	45	41.50
9	112	55	50.72
10	45	45	41.50
11	37	75	69.16
12	108	70	64.55
13	86	45	41.50
14	28	55	50.72
15	88	70	64.55
16	16	30	27.67
17	47	15	13.83
18	102	40	36.89
		TOTAL	848.40

Table 4.6: PVIcQ facility generation in the 20% penetration case.

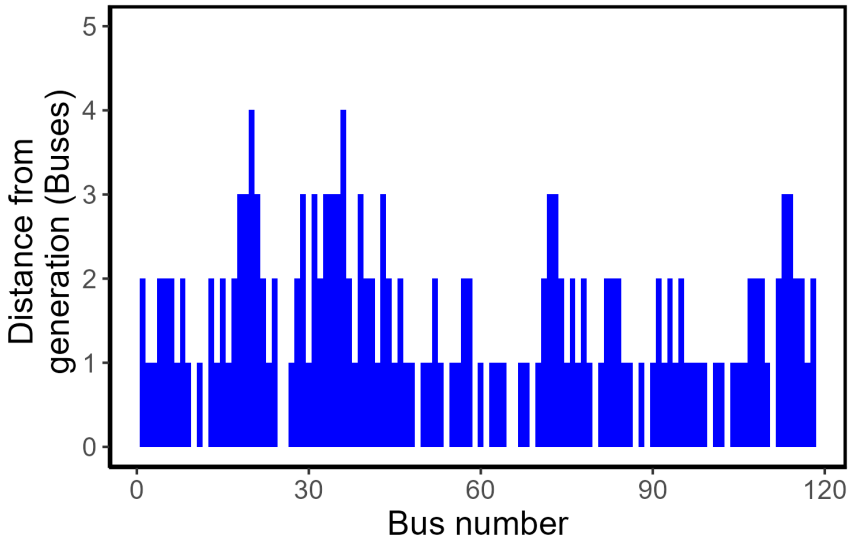

Figure 4.4: Distance between each bus in the modified test system from the nearest point of generation in the base case containing no PV generation.

generation before the addition of any PV facility. As the level of PV penetration increases, this distance from generation changes to include the active PV facilities and exclude the removed traditional generation. With increasing penetration levels, there is a large initial change in these distances as the PV facilities are set to produce active power and as the penetration continues to increase, the distances will change as traditional generation is removed to accommodate the increasing PV generation. Fig.4.5 shows the both distances at 10% penetration and the change in distance from the base case of no PV and demonstrates the large initial change in the distances. Fig.4.6 shows the both distances at 20% penetration and the change in distance from the base case of no PV and demonstrates the the smaller changes due to the incremental removal of traditional generation with increasing PV.

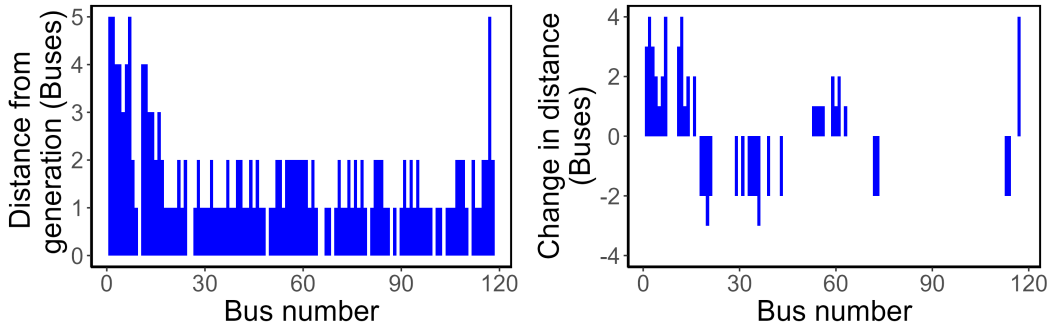

(a) (b)

Figure 4.5: (a) Distance between each bus and the nearest point of generation and (b) change in the distance when compared to the base case of no PV for the case of 10% penetration

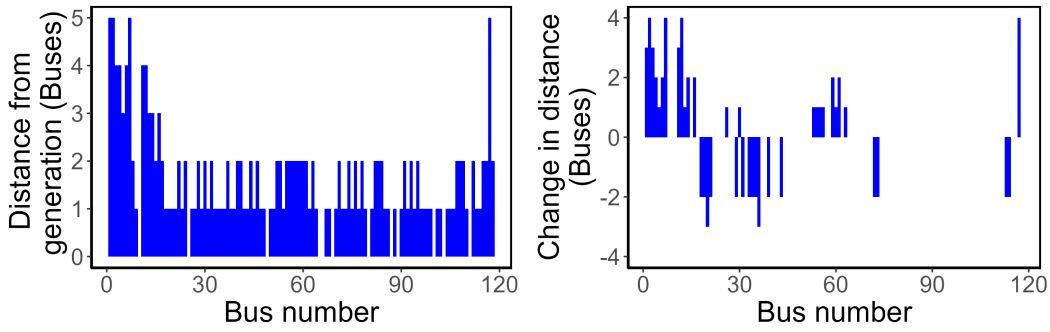

(a) (b)

Figure 4.6: (a) Distance between each bus and the nearest point of generation and (b) change in the distance when compared to the base case of no PV for the case of 20% penetration

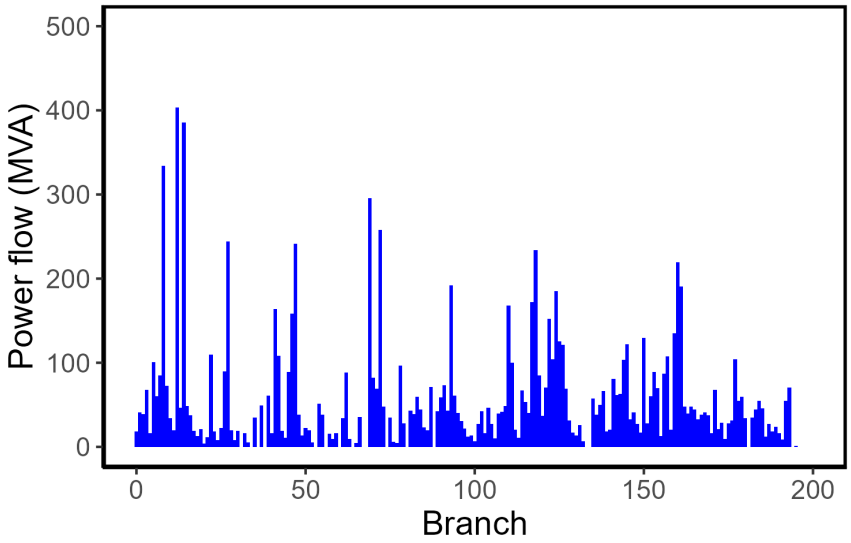

Figure 4.7: Power flow through each transmission line and transformer in the modified test system in the base case containing no PV generation.

Penetration (%)	Avg. Distance (Buses)	Avg. Power Flow (MVA)
0	1.458	55.384
10	1.551	61.466
20	1.568	59.449

Table 4.7: Average distances between a bus and the nearest point of generation compared to the average MVA flow in transmission lines and transformers.

The power flow in each ot the transmission lines and transformers was recorded at each level. Fig.4.7 shows the power flow in MVA through each transmission line and transformer in the network before the addition of any PV facility. Fig.4.5 shows both the power flow at 10% penetration and the change in power flow from the base case. Fig.4.6 shows both the power flow at 20% penetration and the change in power flow from the base case of no PV.

The voltage at each bus was recorded at each penetration level. Fig.4.10 shows the

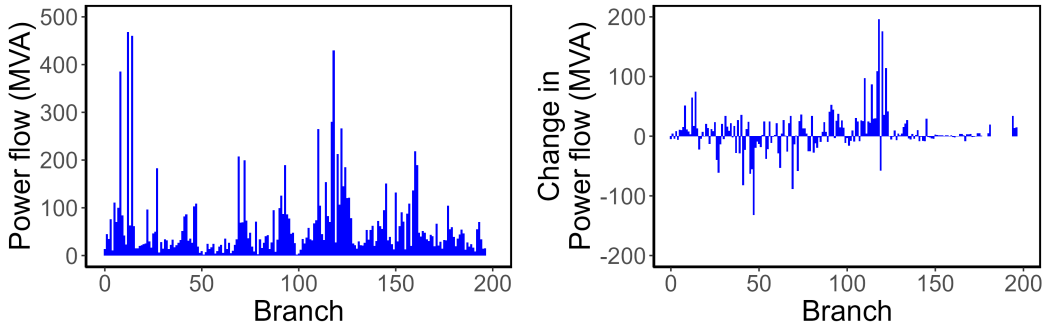

(a) (b)

Figure 4.8: (a) Power flow through each transmission line and transformer and (b) change in the power flow when compared to the base case of no PV for the case of 10% penetration

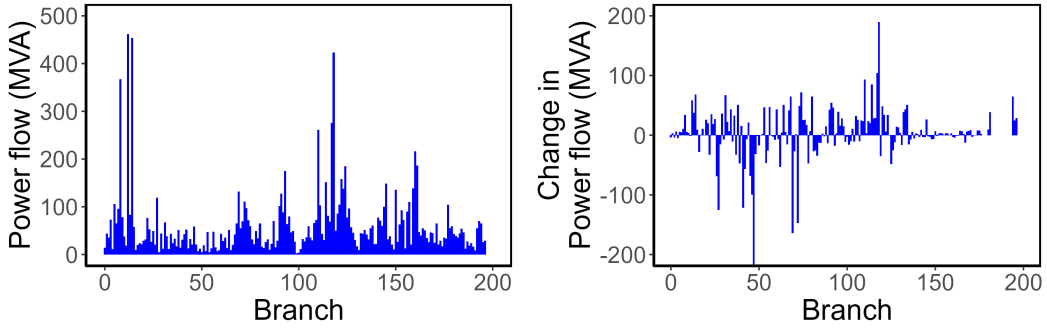

(a) (b)

Figure 4.9: (a) Power flow through each transmission line and transformer and (b) change in the power flow when compared to the base case of no PV for the case of 20% penetration

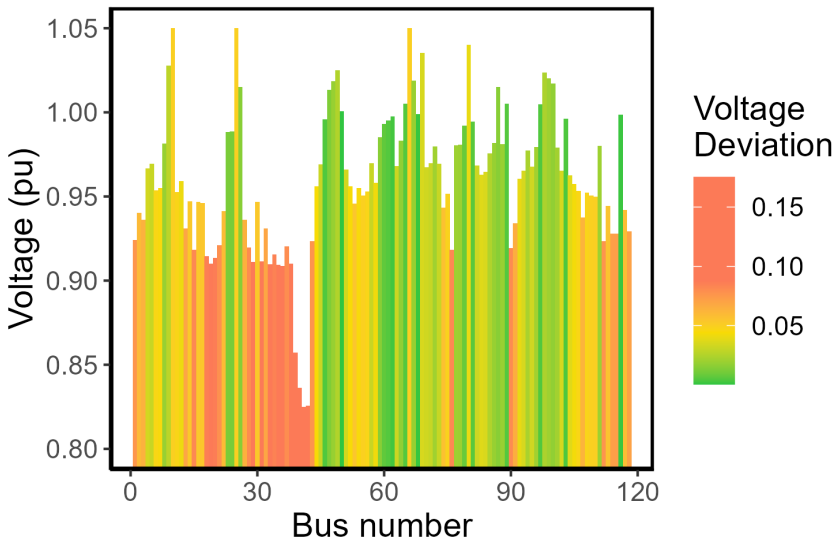

Figure 4.10: Voltage at each bus in the modified test system in the original base case without PV generation. Note the low voltages purposefully included in the test case specification.

voltage in per-unit at each bus in the network before the addition of any PV facility. Fig.4.11 shows both the voltage at 10% penetration and the change in voltage from the base case. Fig.4.12 shows both the voltage at 20% penetration and the change in voltage from the base case of no PV. Color is used to represent the absolute value of the voltage difference from one per-unit, providing a visual indication of the severity of any voltage violation. The results show that the addition of PV facilities causes the low voltage incidents present in the base case to be reduced slightly and also moved to a different location in the system.

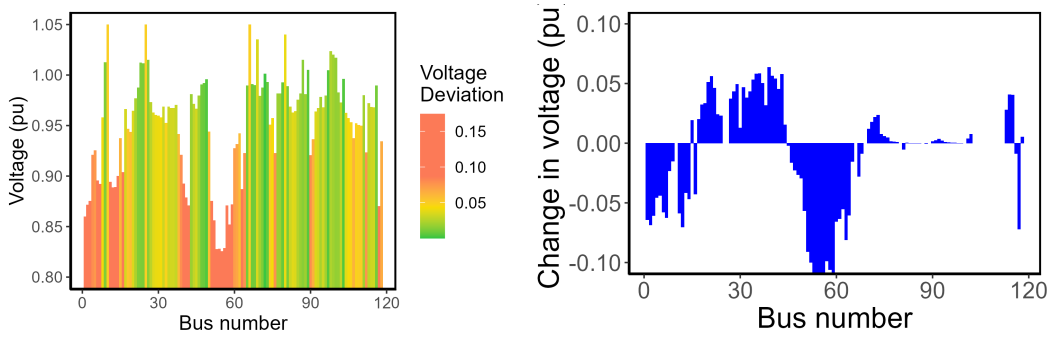

(a) (b)

Figure 4.11: (a) Voltage at each bus and (b) change in the voltage when compared to the base case of no PV for the case of 10% penetration

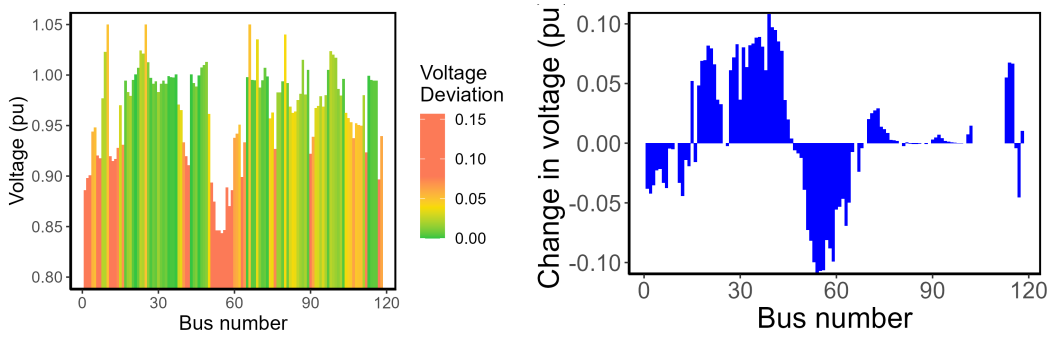

(a) (b)

Figure 4.12: (a) Voltage at each bus and (b) change in the voltage when compared to the base case of no PV for the case of 20% penetration

4.7 Summary

This chapter demonstrates the power flow analysis of a queue of utility-scale solar PV facilities at varying penetration levels on the representative IEEE 118 Bus test system using PSS/E. The additional generation from PV facilities shifts the distribution of generation across the system, changing the distances of load centers to points of generation. As generation is distributed closer to load centers, the required power flow through transmission lines decreases. This results in reduced line loading and power flow losses. The additional PV generation also serves to support the grid voltage, bringing the average voltage level closer to unity with increasing penetration.

Chapter 5

Performance Improvements using Battery Energy Storage (BES)

This chapter discusses the optimization of the location of battery energy storage facilities for voltage support on a representative transmission network containing large-scale PV installations using PSS/E. A battery was connected at points in the system experiencing severe voltage deviations and the effect on the system voltages was measured to select the optimal location for the battery. This was process was iterated to find an optimal combination of installed batteries which effectively reduced the voltage deviation of the system.

5.1 Introduction

Large-scale integration of solar energy resources to the transmission grid poses several challenges of interest. The day-night cycle and weather conditions mean that PV generation is intermittent, and procedures must be put in place to match electric

demand during times of rapid generation change. This is an issue for traditional synchronous generation, whose ramp up rate is typically much longer than the length of periods of sudden shading. Related to load mismatch is inertia, which is the ability of synchronous machines to match demand under conditions of surplus or shortage of generation by drawing energy from the rotation of the machine. This allows for estimation of the necessary input power through frequency monitoring, and also some leniency in the acceptable amount and duration of power mismatch. Without energy storage in a rotational system, photovoltaic sources of energy have no inertia[31]. High levels of PV penetration would result in less leniency in power mismatch. In a system consisting of only PV, the input solar power must be equal to the demand at every instance to avoid grid failure. Finally, the range of power factors used by traditional generation allow for reactive power to be absorbed and injected as needed. This provides support to the by maintaining adequate voltage levels. The total solar generation integrated into the grid must then be able to supply enough reactive power to support grid voltage as it replaces traditional forms of generation.

Battery energy storage provides a way to offset the challenges associated with PV deployment. During periods of generation intermittency, the battery would be able to discharge when there is a shortage of power and charge when there is a surplus, lowering the total power mismatch due to rapid changes in the generation profile. BES systems can switch on rapidly. The ability of the battery systems to be dispatched

quickly and the support they provide to the power mismatch allow them to mitigate the decrease in system inertia. Finally, battery systems provide an additional point of generation where reactive power can be supplied or absorbed, allowing for the support of grid voltage.

5.2 Addition of BES System

Three components are added to the PSS/E model to model the interconnection of the battery systems. The first component added to the network spreadsheet is the dedicated battery bus. Two parameters for the bus must be specified: the rated voltage and the bus code. The rated voltage for all interconnected battery buses was set to be 13.2 kV. The bus code for these buses was set to two, representing a generator bus, or P-V bus since both active power and voltage are specified for these buses, in steady-state load flow analysis. For added security in the ability of the solver to find a solution, the angle of the bus was also initialized to be the same value as the angle of the bus of interconnection. By default, PSS/E initializes the angle to zero. Large differences in angle between buses represents a large flow of active power, which may lead to a large power mismatch and the inability of the solver to determine a solution.

The next component is the machine representing the electricity generation of the battery. Several machine parameters must be specified for the PV generators. The

main quantities for load flow analysis are the scheduled voltage output of the generator and the active power output. The scheduled voltage was set to 1 pu and the active power output set to the rating of the battery. The source impedance of the machine was also specified. For the PV installations, the source resistance was set to 0 pu and the source reactance set to a large value of 9999 pu.

The final component to be added is the transformer link to the point of interconnection. The resistance and reactance of the transformers were specified. For the battery transformers, the resistance was set to 0.001690 pu and the reactance to 0.070440 pu.

5.3 Battery Location Study

The transmission models of PV penetration developed for study were used to investigate the most suitable location for battery placement in transmission networks with large-scale PV generation facilities. A multi-step, systematic parametric study was performed with a view at optimally minimizing the number of voltage deviation events.

For each of the PV penetration models developed previously, the buses experiencing severe voltage deviations were recorded to test as locations for battery placement. A severe voltage deviation was defined as a voltage value lower than 0.95 per-unit or greater than 1.05 per-unit. Each bus experiencing a violation was connected to a

machine representing a battery energy storage system. The output real power of the battery was set to zero and the scheduled voltage was set to 1 per-unit at the bus of interconnection so that the reactive power output of the machine would be calculated to best stabilize the voltage at the bus. PSS/E was then used to solve the power flow of the system and the resultant voltages of the buses in the system were recorded to evaluate the performance of the battery at the current location. The most suitable bus was selected as the bus which reduced the number of voltage violations the most.

$$argmin(count(V < 0.95 || V > 1.05)) \tag{5.1}$$

This process was repeated for each of the buses and the location was selected to be the bus that reduced the number of voltage deviations the most. This model was then saved and the process was repeated on this model to add a second condenser which would best stabilize the voltages. This process represents a greedy approach, which selects the value that produces the best results at the given iteration.

5.4 Results

The iteration process was completed for the three models of 0, 10, and 20% PV penetration. The optimal location at each iteration was recorded as well as the reactive power output calculated during the iteration and after all batteries had been

Battery Number	Bus Number	Q Gen. Iter. (MVAR)	Q Gen. End (MVAR)	Violations	Change in Violations
0	NA	NA	NA	57	-21
1	19	60.53	38.72	36	-17
2	40	69.82	45.56	19	-8
3	305	25.30	24.59	11	-3
4	76	49.44	49.29	8	-2
5	107	27.36	24.23	6	-2
6	42	44.05	44.04	4	-2
7	90	54.75	54.76	2	-1
8	53	34.31	34.32	1	-1
9	112	38.46	38.47	0	NA

Table 5.1: Summary of battery location iteration results for the case of 0% PV penetration.

placed. The number of violations in during the iteration was recorded to demonstrate the progression of the algorithm. The difference between the violations in two iterations was recorded to represent the marginal benefit of the additional battery.

The base case with no PV generation is demonstrated first in both tabular and graphical form. The summary of the results for this case is shown in Table5.1. The system has 57 buses experiencing severe voltage deviations. The iterative process connects nine batteries across the system to bring the number of violations to zero. The reactive power output after all batteries were added results in either significant decreases in power output or little change. This suggests that additional batteries provide a secondary benefit of reduction of the reactive power requirement of other batteries across the system.

The resulting curve of the number of violations versus the number of batteries

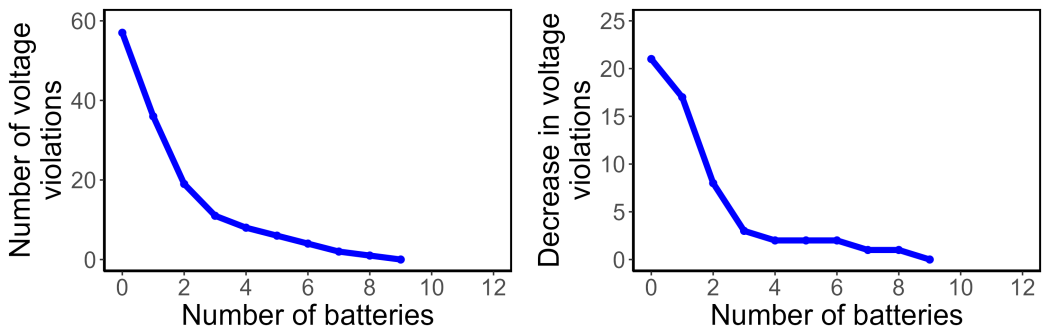

(a) (b)

Figure 5.1: (a) The relationship between the number of batteries and the number of voltage violations and (b) its forward difference for the case of 0% PV penetration.

shown in Fig. 5.1a is approximately a decaying exponential. Thus, we would expect the approximate slope calculated as the difference between adjacent iterations to take the form of an approximately decaying exponential, which is what is seen in Fig.5.1b. This mean that the marginal benefit of an additional battery decreases as more batteries are added.

The summary table of the case of 10% penetration in Table 5.2 shows a decrease in the initial number of violations with 45 violations. This suggests that the addition of PV generation to the system proves beneficial to the voltage stability. Twelve total batteries were required to bring the number of violations to zero. As in the 0% penetration case, the reactive power output of each battery after all batteries are connected is significantly lower than than the output during the iteration, meaning additional batteries reduce the required output from other batteries.

Battery Number	Bus Number	Q Gen. Iter. (MVAR)	Q Gen. End (MVAR)	Violations	Change in Violations
0	NA	NA	NA	45	-10
1	41	51.294	29.197	35	-8
2	12	68.069	45.247	27	-5
3	1	46.782	46.149	22	-4
4	52	58.811	46.149	18	-4
5	55	87.083	46.149	14	-4
6	56	62.850	56.907	10	-2
7	107	27.360	24.232	8	-2
8	76	47.837	47.722	6	-2
9	90	53.824	53.830	4	-2
10	63	60.893	60.909	2	-1
11	42	32.684	32.689	1	-1
12	112	38.461	38.461	0	NA

Table 5.2: Summary of battery location iteration results for the case of 10% PV penetration.

Similar to the case of 0% penetration, the resulting curve of the number of violations versus the number of batteries shown in Fig.5.2a is approximately a decaying exponential. In this case, however, the curve has a slightly closer to linear behavior than the previous case. This results in the graph of Fig.5.2b, which has periods of near constant slope, or marginal benefit. This means that the marginal benefit of an additional battery decreases as more batteries are added, however, there are periods where the benefit is not affected by the addition of a battery.

The summary table of the case of 20% penetration in Table5.2 continues the trends demonstrated in the first two cases. The initial number of violations decreased to 36 violations from the 45 in the previous case, suggesting, again, that the addition of PV generation benefits voltage stability. Twelve total batteries were required to

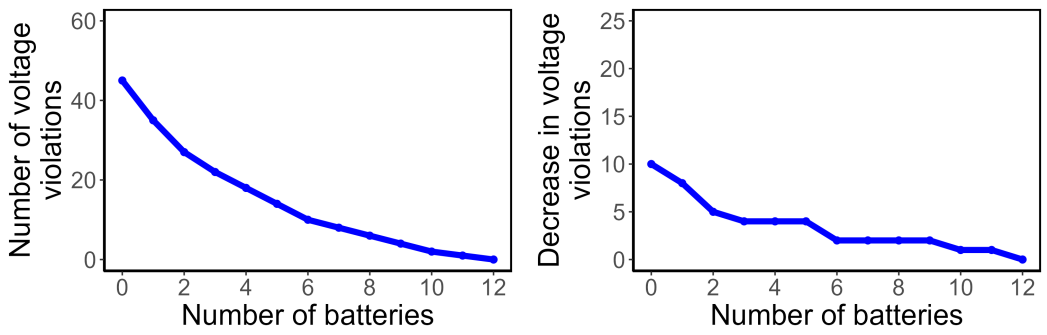

(a) (b)

Figure 5.2: (a) The relationship between the number of batteries and the number of voltage violations and (b) its forward difference for the case of 10% PV penetration.

bring the number of violations to zero. This number was not did not change from the previous case. As in the both previous cases, the reactive power output of each battery after all batteries are connected is significantly lower than than the output during the iteration, meaning additional batteries reduce the required output from other batteries.

In this case, the trend of approaching a linear relationship between the number of violations and number of batteries continues as shown in Fig.5.3a. The graph has a slight drop initially followed by an approximately linear plot. This results in the graph of Fig.5.3b, which has a nearly constant slope, or marginal benefit outside of the initial drop. This means that the marginal benefit of an additional battery decreases as more batteries are added, however, in this case, the benefit is nearly independent of the number of batteries connected.

Battery Number	Bus Number	Q Gen. Iter. (MVAR)	Q Gen. End (MVAR)	Violations	Change in Violations
0	NA	NA	NA	36	-10
1	1	57.605	48.773	26	-4
2	58	68.410	29.590	22	-3
3	117	25.364	25.047	19	-3
4	41	40.003	39.873	16	-3
5	53	53.242	33.504	13	-2
6	107	27.360	24.232	11	-2
7	118	41.612	41.516	9	-2
8	90	52.880	52.886	7	-2
9	59	64.889	41.336	5	-3
10	55	61.581	57.869	2	-1
11	112	38.461	38.467	1	-1
12	63	52.067	52.067	0	NA

Table 5.3: Summary of battery location iteration results for the case of 20% PV penetration.

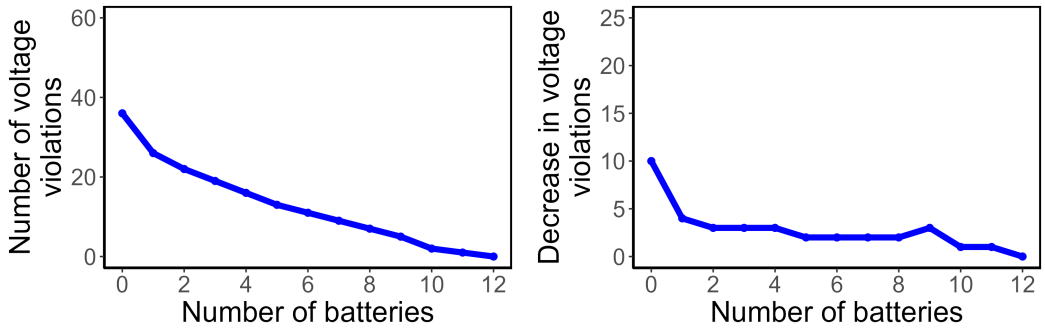

(a) (b)

Figure 5.3: (a) The relationship between the number of batteries and the number of voltage violations and (b) its forward difference for the case of 20% PV penetration.

5.5 Summary

This chapter demonstrates the implementation and results of the use of a greedy, iterative approach in determining the optimal location of battery energy storage systems for grid voltage support. The algorithm selects the single location that most reduces bus voltage violations system wide and repeats this process until the number of violations is minimized.This process was performed on three transmission models representative of various levels of PV penetration to determine trends in relationships between the number of batteries, the number of voltage violations, and the level of PV penetration. In all cases, several trends of interest were seen and are summarized in Fig.5.4.

1. The addition of one battery system reduces the marginal benefit of another battery.

2. Increasing PV penetration results in a decrease in the number of voltage violations across the system, stabilizing voltage levels.

3. Increasing PV penetration results in the relationship between the number of batteries and the number of violations shifting from a decaying exponential to a negative linear relationship; In higher levels of penetration, the marginal benefit is nearly constant.

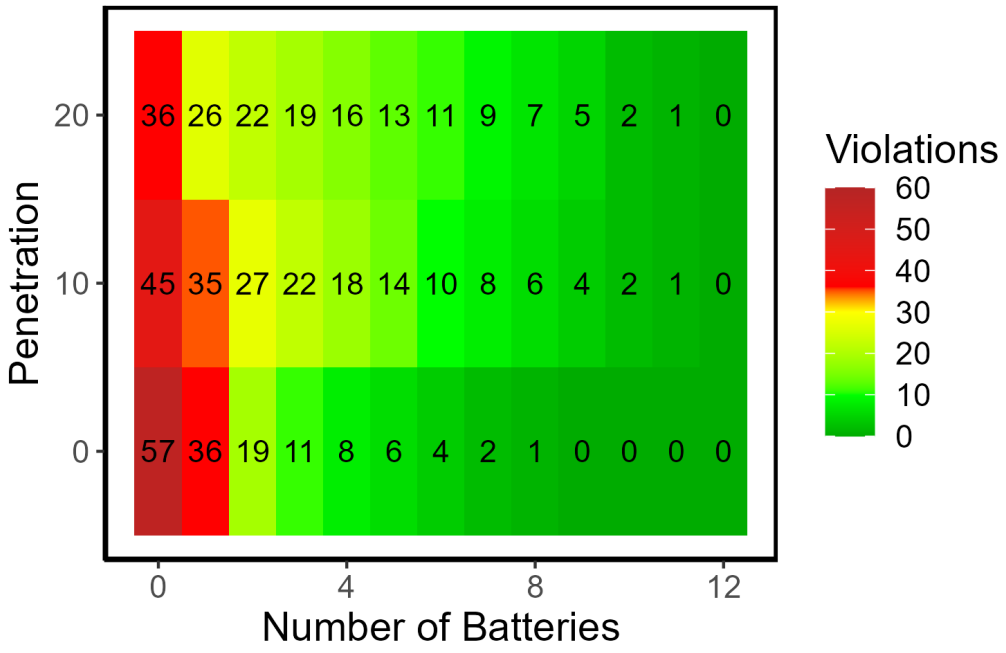

(a)

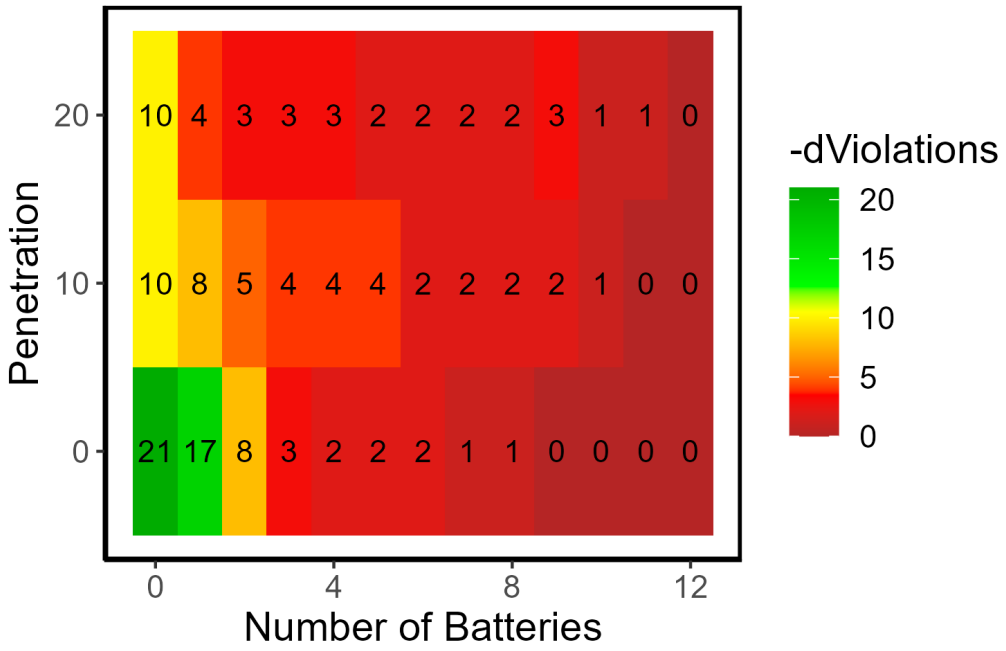

(b)

Figure 5.4: Summary of battery location study results(a) Number of violations (b) Decrease in violations.

4. Additional batteries provide an additional benefit of reducing the required reactive power injection of previously integrated batteries.

Chapter 6

Conclusions and Future Work

6.1 Conclusion

This thesis presents studies investigating the grid addition of utility-scale solar PV installations and battery energy storage systems. The IEEE 118-Bus test case was simulated using PSS/E to assess the impact of PV penetration and battery location on a generic transmission system for generalization to real transmission networks. Chapter one introduced the background and problem formulation for the research performed as well as recent work related to the area of study. Chapter two presents the theory and mathematical algorithms and representations that are used to model power system components.

Chapter three describes the algorithms used to simulate power flow and relates the theoretical formulas to the software and automation used to complete the studies. Several scripting tools were developed using Python for the automation of the creation of transmission models of varying PV penetration, the optimization of battery

location for voltage support, and the collection, organization, and visualization of data gathered from the power flow solution.

Chapter four presents the simulation of utility-scale solar PV interconnection to a representative transmission network. The PVIcQ was developed and connected to the test network. The output power of the solar facilities was increased to assess the impact of PV penetration level, which may be applied to real transmission systems. The additional PV facilities was found to alter the distribution of generation, resulting in variation in the distances between generators and load centers. Increases in the distance between generation and load was found to increased line loading. Incorporation of additional PV generation also resulted in decreases in voltage deviations from unity.

Chapter five demonstrates the deployment of an optimization algorithm to determine the location of battery energy storage facilities for voltage support on the transmission models developed in chapter four. An iterative process was developed and employed to connect the single battery which produces the highest benefit at that step and steps until the voltage violations were minimized. This process was performed models of varying PV penetration to examine the relationships between the number of batteries, the number of voltage violations, and the level of PV penetration. Several trends were realized over the three models tested. Connecting a

battery to the network decreases the marginal benefit of the addition of the next battery. Increases in PV generation level resulted in decreases in the number of voltage violations. Increasing the PV generation resulted in linearization of the relationship between the number of batteries and voltage violations. This means higher PV penetration levels will have a near constant marginal benefit for additional batteries. The addition of batteries decreases the required reactive power generation from previously connected batteries.

6.2 Original Contributions

A summary of the original contributions developed in this work can be enumerated in the following:

1. The development of a systematic, automated procedure for the integration of PV and BESS installations into th electric power transmission network. The procedures streamline the process of creating network models of PV integration, optimizing the integration of BESS, and simulating and gathering results from PSS/E. Python software was developed alongside these procedures for automation of generation deployment and model creation (Chapter 3)

2. Grid Analysis of impact for different PV penetration levels. The analysis quantified the important relationship between the distributed nature of additional utility-scale generation and power flow in the system (Chapter 4).

3. The development of an optimization method for BESS location and rating to provide voltage support. The algorithm searches a realistic subsection of the location space and provides a locally optimal solution for voltage support (Chapter 5).

6.3 Future Work

The importance of the simulation of transmission level solar PV impact was discussed. Much of the recent work in PV impact analysis focuses on distribution analysis of residential PV installations. As the adoption rate of residential PV and the interest in multi-megawatt scale PV facilities increase, the need for studies of impact at the transmission level grows. Future work could include investigations of the effect of PV on both levels. Cosimulation of transmission and distribution systems could analyze the local and regional effect of large scale residential PV that may propagate to the transmission level. Studies could also investigate the combined effect of residential PV and utility-scale systems.

The steady-state impact of large-scale PV facilities was demonstrated. Steady-state analysis allows the complex models of the power electronics necessary for PV operation to be simplified into a model representing the ateady-state operation. Future studies can investigate the dynamic and transient behavior of such PV systems

and its effect on transmission system operation. Conditions such as sudden complete or partial shading an be analyzed for both dynamic stability such as rotor angle stability and transient stability.

Optimization of battery location for grid voltage support was developed and presented. Future work can examine location optimization using an expanded objective function which takes into account cost, voltage, power flow, or other factors. Other methods of optimization such as differential evolution may be explored and their results compared. In addition to battery location, battery sizing optimization may be explored.

References

[1] O. M. Akeyo, "Analysis and Simulation of Photovoltaic Systems Incorporating Battery Energy," MSc thesis, University of Kentucky, 2017.

[2] P. Fernandez-Porras, M. Panteli, and J. Quiros-Tortos, "No Title," *IET Generation, Transmission & Distribution*, vol. 12, 2018.

[3] Wikipedia, "Gradient Descent," 2021. [Online]. Available: https://en.wikipedia.org/wiki/Gradient{_}descent

[4] M. Al-Saffar, S. Zhang, A. Nassif, and P. Musilek, "Assessment of Pgotovoltaic Hosting Capacity of Existing Distribution Circuits," in *IEEE Canadian Conference of Electrical and Computer Engineering*. Edmonton, Canada: IEEE, 2019.

[5] B. B. Navarro and M. M. Navarro, "A Comprehensive Solar PV Hosting Capacity in MV and LV Radial Distribution Networks," in *IEEE PES Innovative Smart Grid Technologies Conference Europe*. Turin, Italy: IEEE, 2017.

[6] R. Torquato, D. Salles, C. O. Pereira, P. C. M. Meira, and W. Freitas, "A Comprehensive Assessment of PV Hosting Capacity on Low-Voltage Distribution Systems," *IEEE Transactions on Power Delivery*, vol. 33, no. 2, pp. 1002–1012, 2018.

[7] M. U. Qureshi, A. Kumar, S. Grijalva, J. Deboever, J. Peppanen, and M. Rylander, "Fast Hosting Capacity Analysis for Thermal Loading Constraint Using Sensitivity-Based Decomposition Method," in *52nd North American Power Symposium (NAPS)*. Tempe, USA: IEEE, 2021.

[8] S. Wang, Y. Dong, L. Wu, and B. Yan, "Internal Overvoltage Risk Based PV Hosting Capacity Evaluation Considering PV and Load Uncertainties," *IEEE Transactions on Smart Grid*, vol. 11, no. 3, pp. 2709–2721, 2020.

[9] M. S. S. Abad and J. Ma, "Photovoltaic Hosting Capacity Sensitivity to Active Distribution Network Management," *IEEE Transactions on Power Systems*, vol. 36, no. 1, pp. 107–117, 2021.

[10] A. Kaneko, Y. Hayashi, T. Anegawa, H. Hokazono, and Y. Kuwashita, "Evaluation of an Optimal Radial-Loop Configuration for a Distribution Network with PV Systems to Minimize Power Loss," *IEEE Access*, vol. 8, pp. 220 408–220 421, 2020.

[11] G. Kou, J. Jordan, B. Cockerham, R. Patterson, and P. VanSant, "Negative Sequence Current Injection of Transmission Solar Farms," *IEEE Transactions on Power Delivery*, vol. 35, no. 6, pp. 2740–2743, 2020.

[12] V. Rallabandi, O. M. Akeyo, and D. M. Ionel, "Modeling of a Multi-Megawatt Grid Connected PV System with Integrated Batteries," in *IEEE International Conference on Renewable Energy Research and Applications (ICRERA)*. Birmingham, UK: IEEE, 2016.

[13] H. Jain, B. Palmintier, I. Krad, and D. Krishnamurthy, "Studying the Impact of Distributed Solar PV on Power Systems Using Integrated Transmission and Distribution Models," in *IEEE/PES Transmission and Distribution Conference and Exposition (T&D)*. Denver, USA: IEEE, 2018.

[14] N. Samaan, M. A. Elizondo, B. Vyakaranam, M. Vallem, X. Ke, R. Huang, J. T. Holzer, S. Sridhar, Q. Nguyen, Y. V. Makarov, X. Zhu, J. Wang, and N. Lu, "Combined Transmission and Distribution Test System to Study High Penetration of Distributed Solar Generation," in *IEEE/PES Transmission and Distribution Conference and Exposition (T&D)*. Denver, USA: IEEE, 2018.

[15] D. Bian, M. Kuzlu, M. Pipattanasomporn, S. Rahman, and Y. Wu, "No Title," in *IEEE Power & Energy Society General Meeting*. Denver, USA: IEEE, 2015.

[16] M. Zeraati, M. E. H. Golshan, and J. M. Guerrero, "Distributed Control of Battery Energy Storage Systems for Voltage Regulation in Distribution Networks with High PV Penetration," *IEEE Transactions on Smart Grid*, vol. 9, no. 4, pp. 3582–3593, 2018.

[17] L. Held, M. Armbruster, M. Zimmerlin, M. R. Suriyah, T. Leibfried, and R. Höche, "The Operation of a Battery Storage Ssytem to Avoid Overvoltages in a Low Voltage Grid," in *6th IEEE International Energy Conference (ENERGYCon)*. Gammarth, Tunisia: IEEE, 2020.

[18] V. Rallabandi, O. M. Akeyo, N. Jewell, and D. M. Ionel, "Incorporating Battery Energy Storage Systems Into Multi-MW Grid Connected PV Systems," *IEEE Transactions on Industry Applications*, vol. 55, no. 1, pp. 638–647, 2018.

[19] S. B. Q. Naqvi and B. Singh, "An Improved Power Quality PV-Battery System Coupled to Weak Grid with Feed-in Tariff Flexibility and PV Intermittency Flattening," in *IEEE 5th International Conference on Computing Communication and Automation (ICCCA)*. Greater Noida, India: IEEE, 2020.

[20] U. Sohail, H. Nademi, and L. E. Norum, "A Reliable Modular Based PV-Battery

Hybrid System with Peak Shaving Capability," in *IEEE 19th Workshop on Control and Modeling for Power Electronics (COMPEL)*. Padua, Italy: IEEE, 2018.

[21] P. Kolte and V. Mohale, "Improved System Of Constant Power Generation In Grid Connected PV Cell With Battery," in *2nd International Conference on Intelligent Computing, Instrumentation and Control Technologies (ICICICT)*. Kannur, India: IEEE, 2019.

[22] S. Hashimoto, T. Yamamoto, K. Nara, and N. Tobaru, "Capacity Determination of the DC-side Battery for Hybrid Batteries in PV Generation System," in *IEEE Innovative Smart Grid Technologies - Asia (ISGT Asia)*. Chengdu, China: IEEE, 2019.

[23] M. Alramlawi and P. Li, "Design Optimization of a Residential PV-Battery Microgrid With a Detailed Battery Lifetime Estimation Model," *IEEE Transactions on Industry Applications*, vol. 56, no. 2, pp. 2020–2030, 2020.

[24] A. Z. Gabr, A. A. Helal, and N. H. Abbasy, "Multiobjective Optimization of Photo Voltaic Battery System Sizing for Grid-Connected Residential Prosumers Under Time-of-Use Tariff Structures," *IEEE Access*, vol. 9, pp. 74 977–74 988, 2021.

[25] R. Khezri, A. Mahmoudi, and M. H. Haque, "Optimal Capacity of Solar PV and Battery Storage for Australian Grid-Connected Households," *IEEE Transactions on Industry Applications*, vol. 56, no. 5, pp. 5319–5329, 2020.

[26] O. M. Akeyo, V. Rallabandi, N. Jewell, and D. M. Ionel, "The Design and Analysis of Large Solar PV Farm Configurations With DC-Connected Battery Systems," *IEEE Transactions on Industry Applications*, vol. 56, no. 3, pp. 2903–2913, 2020.

[27] Y. Huang, "Day-Ahead Optimal Control of PEV Battery Storage Devices Taking Into Account the Voltage Regulation of the Residential Power Grid," *IEEE Transactions on Power Systems*, vol. 34, no. 6, pp. 4154–4167, 2019.

[28] M. O. Badawy and Y. Sozer, "Power Flow Management of a Grid Tied PV-Battery System for Electric Vehicles Charging," *IEEE Transactions on Industry Applications*, vol. 53, no. 2, pp. 1347–1357, 2017.

[29] J. Glover, T. J. Overbye, and M. S. Sarma, *Power System Analysis & Design*, 3rd ed. Cengage Learning, 2017.

[30] S. Dimitrijev, *Principles of Semiconductor Devices*, 2nd ed. New York: Oxford University Press, 2012.

[31] J. Fang, H. Li, Y. Tang, and F. Blaabjerg, "On the Inertia of Future More-Electronics Power Systems," *IEEE Journal of Emerging and Selected Topics in Power Electronics*, vol. 7, no. 4, pp. 2130–2146, 2018.

[32] Y. Zhang, X. Liu, Y. Wu, S.-e. Wang, Y. Wang, Z. Tang, H. Zheng, and J. Hao, "Analysis of Inertia Mechanism of Grid-tied Photovoltaic Power Generation System with Virtual Inertia Control," in *4th IEEE Workshop on the Electric Grid (eGRID)*. Xiamen, China: IEEE, 2019.

[33] G. Yan, X. Zhang, S. Zhang, and H. Yang, "A Novel Virtual Inertial Control Strategy for Double Stage PV Generation," in *2nd Conference on Energy Internet and Energy System Integration*. Beijing, China: IEEE, 2018.

[34] S. K. Togiti, "Comparative Analysis of Load Flow Techniques for Steady State Loading Margin and Voltage Stability Improvement of Power Systems," MSc thesis, University of New Orleans, 2015.

[35] SIEMENS, "PSSE 33.5 - Program Applications Guide Volume 1," Schenectady, USA, 2013.

[36] R. Vykuka and L. Noháčová, "Fast-Decoupled Method for Contingency Analysis," in *15th International Scientific Conference on Electric Power Engineering (EPE)*. Brno-Bystrc, Czech Republic: IEEE, 2014.

[37] B. Stott, "Review of Load-Flow Calculation Methods," *Proceedings of the IEEE*, vol. 62, no. 7, pp. 916–929, 1974.

[38] B. Karlsson, "Comparison of PSSE & PowerFactory," Thesis, Uppsala University, 2013.

[39] U.S. Energy Information Administration, "Monthly Energy Review," U.S. Energy Information Administration, Washington, Tech. Rep., 2021.

[40] R. Christie, "118 Bus Power Flow Test Case," 1993. [Online]. Available: https://labs.ece.uw.edu/pstca/pf118/pg{_}tca118bus.htm

[41] I. Peña, C. B. Martinez-Anido, and B.-M. Hodge, "An Extended IEEE 118-Bus Test System With High Renewable Penetration," *IEEE Transactions on Power Systems*, vol. 33, no. 1, pp. 281–289, 2018.

[42] NERC, "Reactive Power Planning - Reliability Guideline," NERC, Atlanta, USA, Tech. Rep., 2016.

Vita

Gerald Bankes, Master Student

Department of Electrical and Computer Engineering, University of Kentucky

---

EDUCATION

Master of Science - Electrical and Computer Engineering December 2021
University of Kentucky
Thesis: Analysis and Simulation of Photovoltaic Systems Incorporated with Battery Energy Storage
Director of Thesis: Dr. Dan M Ionel

Bachelor of Science - Electrical and Computer Engineering May 2020
University of Kentucky

AWARD AND RECOGNITION

University of Kentucky College of Engineering
Thomas W. Lester Scholarship Recipient

EMPLOYMENT HISTORY

Research Assistant	2020.08 - Present
University of Kentucky	
Teaching Assistant	2020.08 - Present
University of Kentucky	
Student Engineer	2017.04 - 2020.08
East Kentucky Power Cooperative	